

KERR HYSTERESIS CURVES
OF THIN FILM NICKEL-
IRON GRATINGS

THESIS

Presented to the Graduate Council
Of Texas State University-San Marcos
in Partial Fulfillment
of the Requirements

for the Degree

Master of SCIENCE

By

Jett D. Hendrix, B.S.

San Marcos, Texas
May 2004

ACKNOWLEDGEMENTS

I would first like to thank my fiancée Stefanie for all of the support and patience that she has shown while I was working to complete my degrees. She was there to push me when I needed it and she has been my best friend. I love you Stef. I would also like to thank my parents, Paul and Sharon Hendrix, for their support and giving good advice to help me to achieve my goals in life and to help get me where I am today. I love both of you very much. I would also like to thank my brother Paul Jr. and my sister Shelly for their help and being there when I needed them. I love y'all too. I would also like to thank Mr. and Mrs. Larry and Willaine Scheierman for all of their help and support while I have been completing my degrees. Thank you very much; I love you.

I would like to thank Dr. Geerts for all of his help throughout all of my studies here at Texas State University-San Marcos as well as this thesis. He was there for me every time I needed his help. I enjoyed every moment of it. I would also like to thank Dr. Olson for serving on my committee and for giving me the spark and drive to pursue physics as a profession and a passion. I would also like to think Dr. Spencer for his help during my studies and for serving on my committee.

This manuscript was submitted on April 9, 2004.

TABLE OF CONTENTS

	Page
ACKNOWLEDGEMENTS.....	iii
LIST OF FIGURES.....	vi
 CHAPTER	
1 INTRODUCTIONI.....	1
1.1 The Hysteresis Curve.....	2
2 THIN FILM NICKEL-IRON GRATING SAMPLES.....	6
2.1 The Creation of the Samples.....	6
2.2 The Characterization of the Samples.....	7
3 MAGNETO-OPTICAL KERR EFFECT.....	14
4 MAGNETO-OPTICAL KERR TRACER AND KERR MICROSCOPE..	24
4.1 The Original Kerr Tracer Measurement Technique.....	24
4.2 The Magneto-Optical Kerr Ellipsometer Setup.....	25
4.3 The Kerr Microscope Setup.....	29
5 MAGNETO-OPTICAL KERR TRACER SET-UP TESTING AND PREPARATION.....	33
5.1 Setup Testing.....	33
5.1.1 Retardation Angle.....	34
5.1.2 PEM Rotation Angle Dependence.....	36
5.1.2.1 Separation of the Even and Odd Parts from the Curves.....	41
6 NEW MEASUREMENT RECIPE.....	47
6.1 Selection of the in-plane component of the magnetization.....	47
6.1.1 Longitudinal Magnetization Component.....	49
6.1.2 The Transverse Magnetization Component.....	50
6.2 Non-linear component of the Magnetization.....	52
6.3 The Kerr Microscope Measurement Results.....	53
6.3.1 The Large Grating.....	53
6.3.2 The Medium Grating.....	56

6.3.3 The Small Grating.....	58
7. CONCLUSIONS AND RECOMMENDATIONS.....	62
7.1 Summary and Conclusions.....	62
7.2 Recommendations for Further Research.....	63
7.2.1 Measuring the Medium and Small Grating.....	63
7.2.2 Dependence when the Magnetic Field is Applied Along Easy Axis.....	63
7.2.3 Applying Additional External Stresses.....	64
APPENDIX A.....	65
WORKS CITED.....	75

LIST OF FIGURES

Figure 1.2 Typical Hysteresis Graph [10].....	3
Figure 1.2 Preliminary MO-Kerr Hysteresis curve of a NiFe grating.....	5
Figure 2.1 Profile of the Large Grating [5].....	8
Figure 2.2 Profile of the Medium Grating [5].....	8
Figure 2.3 Profile of the Small Grating [5].....	9
Figure 2.4 Optical Profilometer [13].....	10
Figure 2.5 Thickness Versus X-Direction Raw Data. Optical Profilometer Scan on Sample 102501L01.....	11
Figure 2.6 Profile of the Large Grating.....	11
Figure 2.7 Profile of the Medium Grating.....	12
Figure 2.8 Profile of the Small Grating.....	12
Figure 3.1 Direction of Magnetization.....	14
Figure 3.2 Measurement configuration that is insensitive to components of the magnetization perpendicular to the plane of incidence.....	23
Figure 4.1 The Magneto-Optical Kerr Ellipsometer Setup.....	26
Figure 4.2: Block diagram of the Kerr setup.....	28
Figure 4.3 Two Types of Kerr Microscopes, a) low resolution with high sensitivity, b) High resolution distortion free Kerr microscope [9].....	30
Figure 4.4 Block Diagram of the Kerr Microscope Setup.....	31
Figure 4.5: Domain pattern of sample 10250101: (a) horizontal component of the magnetization; (b) vertical component of the magnetization.....	32
Figure 5.1 The First Three Bessel Functions.....	35
Figure 5.2 Ellipticity Saturation vs. PEM Retardation Angle.....	36
Figure 5.3 MO Kerr Ellipticity hysteresis curves for sample 10280104 for different orientations of the PEM: (a) -45 degrees; (b) -30 degrees; (c) -15 degrees; (d) 15 degrees; (e) 30 degrees; (f) 45 degrees;(g) comparison of all ellipticity curves to show differences in magnitude...38	38
Figure 5.4 MO Kerr rotation hysteresis curves for sample 10280104 for different orientations of the PEM: (a) -45 degrees; (b) -30 degrees; (c) -15 degrees; (d) 15 degrees; (e) 30 degrees; (f) 45 degrees; (g) comparison of all rotation curves to show differences in magnitude...41	41
Figure 5.5 Odd and even parts of the Kerr ellipticity hysteresis curve of sample 10280104 for different orientations of the PEM: (a) -45 degrees; (b) -30 degrees; (c) -15 degrees; (d) 15 degrees; (e) 30 degrees; (f) 45 degrees.....	43
Figure 5.6 Odd and even parts of the Kerr rotation hysteresis curve of sample 10280104 for different orientations of the PEM: (a) -45 degrees; (b) -30 degrees; (c) -15 degrees; (d) 15 degrees; (e) 30 degrees; (f) 45 degrees.....	44
Figure 6.1 New Measurement Setup.....	48
Figure 6.2 Longitudinal hysteresis curve of sample 10280104 (component of the magnetization parallel to the applied field) from the large grating.....	50

Figure 6.3 Transverse hysteresis curve of sample 10280104 (component of the magnetization perpendicular to the applied field) from the large grating.....	51
Figure 6.4 The Large Grating.....	54
Figure 6.5 The Large Grating During Reversal Process.....	55
Figure 6.6 Large Grating Sample # 10250101.....	56
Figure 6.7 Medium Grating With Partially Flipped Strip.....	57
Figure 6.8 Medium Grating Sample # 10250101.....	58
Figure 6.9 Small Grating Sample 10250101 1 st Image.....	59
Figure 6.10 Small Grating Sample 10250101 2 nd Image.....	60
Figure 6.11 Small Grating Sample 10250101 3 rd Image.....	60
Figure 6.12 Small Grating Sample # 10250101.....	61

CHAPTER 1

INTRODUCTION

The use of small thin magnetic films is becoming popular. Two uses of these films are magnetic RAM and read/write heads for magnetic recording. As the thickness and size of these magnetic films decreases, the need for more sensitive magnetic characterization techniques increases.

The magnetic reversal process in magnetic films is usually characterized by a hysteresis curve. This curve is normally measured by a vibrating sample magnetometer, or VSM. The VSM is a good tool to use when there is a large quantity of magnetic material to be tested. Since the amount and size of the magnetic material being used in today's devices is small, this technique is not the best characterization technique.

The magneto-optical Kerr tracer is a much more sensitive technique than the VSM. A Kerr tracer measures the Kerr rotation and the Kerr ellipticity as a function of the applied magnetic field. Since the Kerr effects are linearly proportional to the magnetization in the material, the Kerr hysteresis curves will reflect the magnetic hysteresis of the material.

Another technique that is used to indirectly determine the hysteresis curves is called Kerr microscopy. This technique allows one to see/measure the domain pattern in the material. Once the field dependence of the domain pattern is known, it is possible to calculate the hysteresis curve. This method of Kerr microscopy used is known as Quantitative Kerr Microscopy. This method is applicable to magnetic materials for which the observable magnetization lies basically parallel to the surface and for which the domains are larger than 2 μm . For my project, I used both techniques. The Kerr Microscope and the Kerr tracer are both described in Chapter 4 – Magneto-Optical Kerr Tracer and Kerr Microscope.

1.1 The Hysteresis Curve

The hysteresis curve is a graph of the magnetic moment versus the applied magnetic field. Figure 1.1 shows a typical hysteresis graph [10].

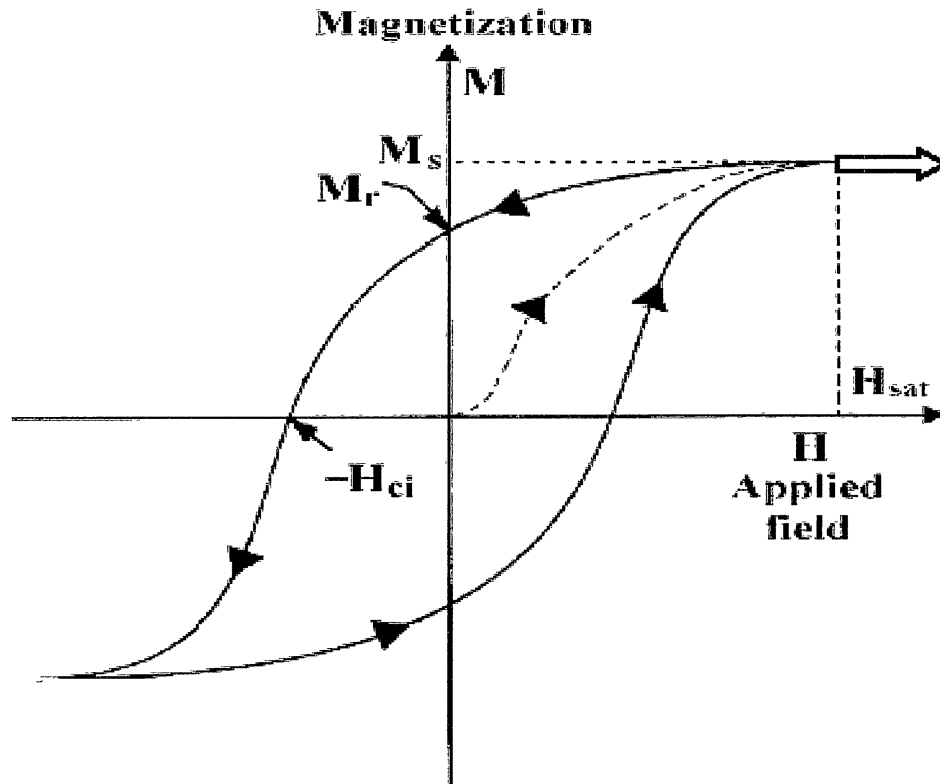


Figure 1.1 Typical Hysteresis Graph [10]

The x-axis shows the applied magnetic field, and the y-axis shows the response of the material, which is called the magnetization. The dashed line originating from the origin shows the path that the magnetization takes when the ferromagnetic sample starts with no remnant magnetization (demagnetized state). When applying a magnetic field, the magnetic spins in the material line up with the field. Once the applied field (H) reaches the saturation field for the material ($=H_{\text{sat}}$) the graph levels off. The material is then said to be in saturation. The magnetization of the material in saturation is called the saturation magnetization (M_s). The dashed curve in Figure 1.1 is sometimes called the virgin magnetization curve

When the applied magnetic field is reduced for a saturated sample, the magnetization curve will be different from the virgin magnetization curve (see Figure 1.1). The magnetization values are higher and at $H_{\text{applied}}=0$, the magnetization is non-zero. This point is labeled as M_r in figure 1.1 and is called the remnant magnetization. The magnetic field is then switched, the poles of the magnets are flipped, and the applied magnetic field is increased in the opposite direction. The point at which the curve crosses the x-axis is labeled $-H_{\text{ci}}$. This point is called the intrinsic coercivity, which is defined as the reverse field required to demagnetize ($M = 0$) the ferromagnetic sample [10]. The reversed field is increased until the sample is once again saturated. The field is then reduced and switched to complete the graph.

The magnetic hysteresis curve of a material can be considered to be the fingerprint of the magnetic material; coercivity, remnant magnetization, and saturation magnetization characterize the magnetic properties of a ferromagnetic material.

This thesis reports on an investigation of the magnetic properties of NiFe gratings using a MO Kerr tracer. Figure 1.2 shows an image of a MO-hysteresis curve measure on a NiFe grating. It is clear the the hysteresis curve is not symmetrical and also shows what looks to be a negative susceptibility. A negative susceptibility is a property of a diamagnetic material. The NiFe sample has a composite of 69% nickel

and 31% iron. Both materials are ferromagnetic materials that have very small diamagnetic properties that can be neglected.

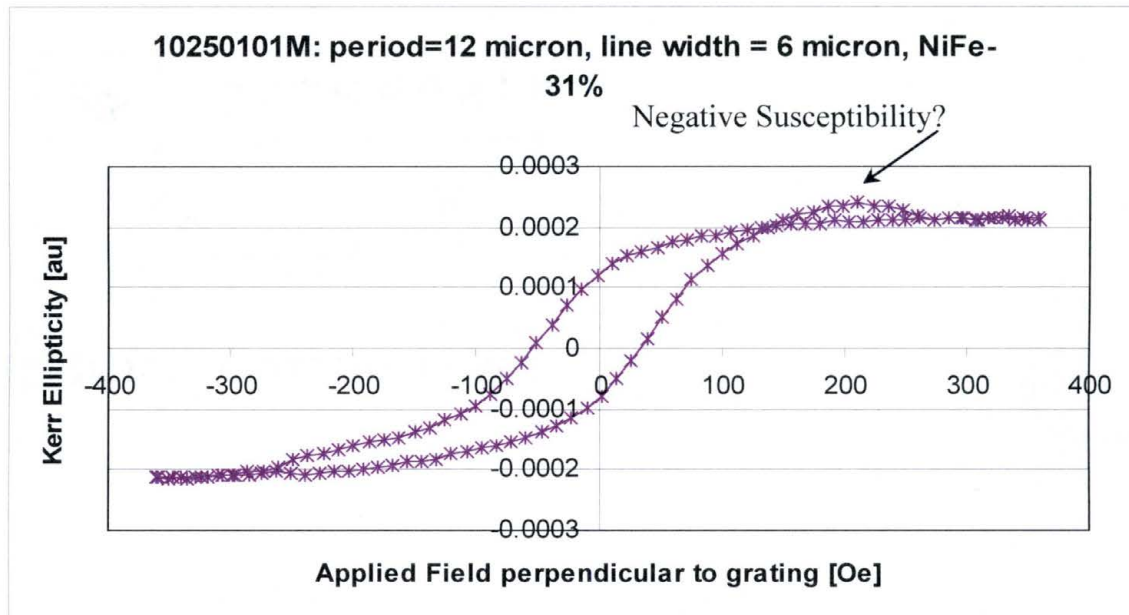


Figure 1.2 Preliminary MO-Kerr Hysteresis curve of a NiFe grating.

This hysteresis curve was obtained using the MO Kerr tracer technique. The MO Kerr tracer technique has been proven to be an acceptable measurement technique for isotropic films. The NiFe grating that we are characterizing, however, is anisotropic. The MO-Kerr tracer technique needs to be adjusted so that these anisotropic microstructures can then be characterized correctly. In this thesis, we develop a new measurement technique. We also investigated the reason for the asymmetric appearance of the hysteresis curves and the reason for the negative susceptibility.

CHAPTER 2

THIN FILM NICKEL-IRON GRATING SAMPLES

In this chapter, I will discuss the creation and characterization of the samples that we used during the course of this thesis. The experiments were done on the following two samples. Sample 10280104 was used for the Kerr rotation experiments, and sample 10250101 was used for the Kerr Microscopy experiments. These samples were made by Claude Garrett and are discussed in more detail in his thesis [5].

2.1 The Creation of the Samples

The samples were sputtered in a DC Magnetron sputtering machine. One-inch silicon wafers were used as a substrate. The silicon wafers had the following parameters: thickness = 0.3mm, $\rho = 1\text{-}20 \Omega \text{ cm}$, p-type, test-grade, (100) orientation, and made by Wafer-world Inc [5]. Two different targets were used for the creation of the samples. The first was a NiFe-45% target, which was used to sputter sample 10280104. The other sample, 10250101, was sputtered using a NiFe-35% target [5]. Once the films were sputtered, Claude Garrett used an argon laser writer

to create different gratings in the thin films. He made three different gratings on each wafer. Their pitch, the distance from the center of one line to the center of the next, was 18 μm for the large grating, 12 μm for the medium grating, and 6 μm for the small grating, with a line width of 9 μm , 6 μm , and 2 μm respectively. More details on how the gratings were produced can be found in the thesis of Claude Garrett [5].

2.2 The Characterization of the Samples

Once the samples were made, they went through some testing to ensure their thickness and check their quality. One setup that was used to check the line thickness and the pitch of the gratings was the stylus profilometer in Dr. Gutierrez' lab. The profilometer consists of a small sharp stylus that is kept at a constant force as it is dragged across the surface of the sample. The height of the stylus is recorded in a one-dimensional profile plot. Figures 2.1, 2.2, and 2.3 show the topography of the large, medium, and small grating in sample 10250101 [5].

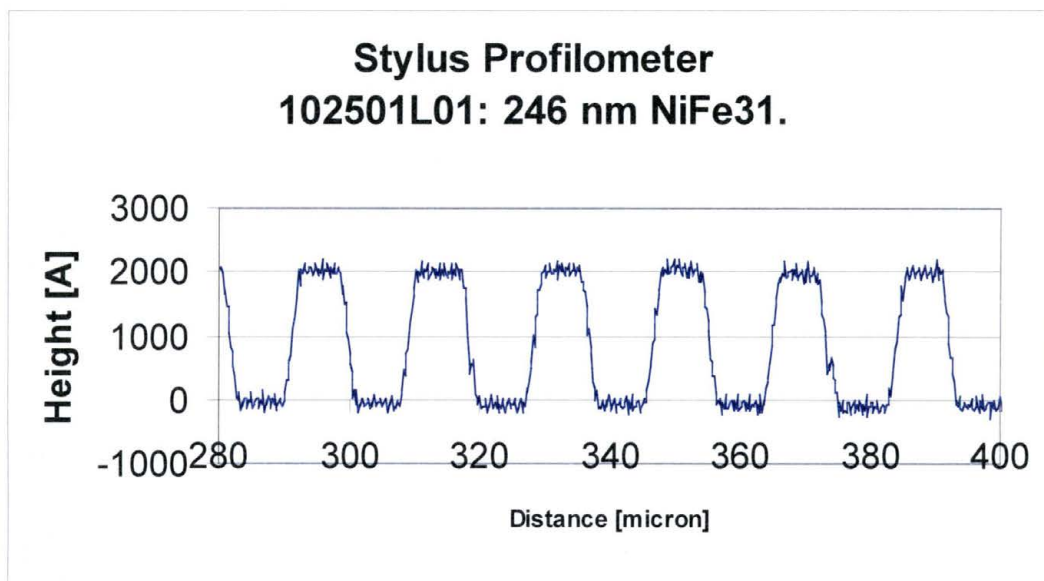


Figure 2.1 Profile of the Large Grating [5]

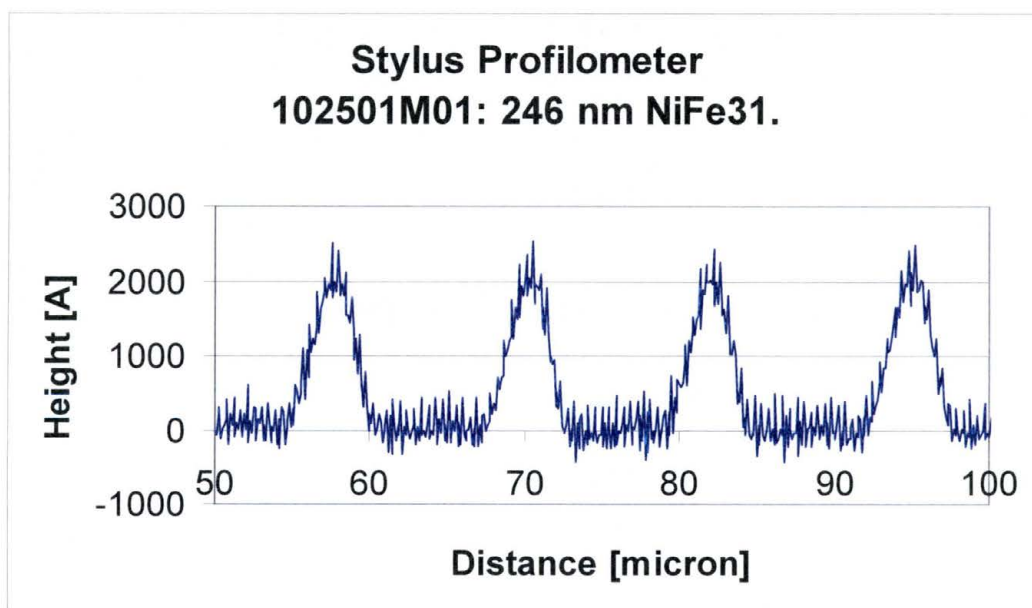


Figure 2.2 Profile of the Medium Grating [5]

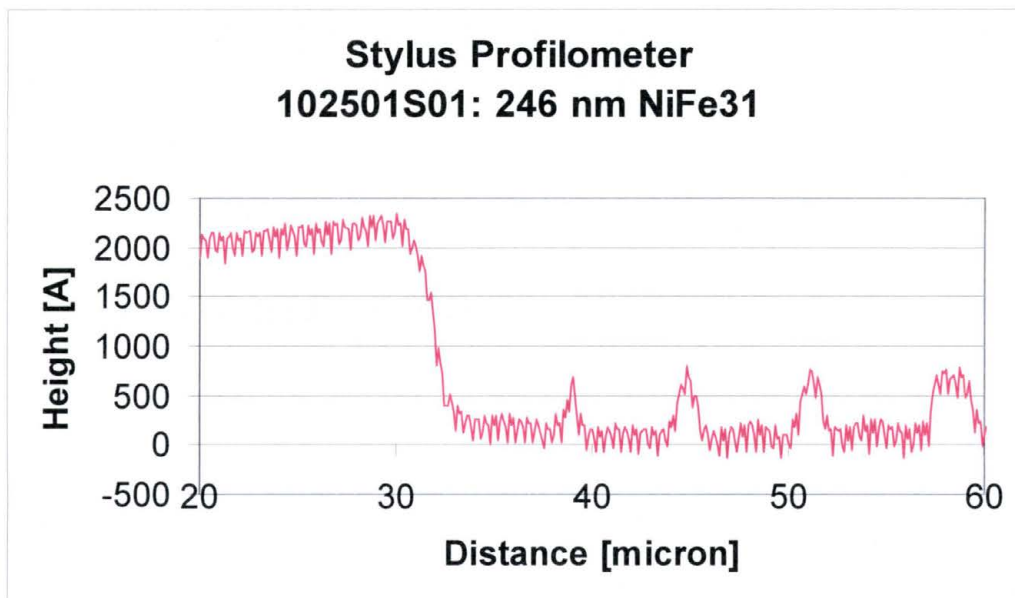


Figure 2.3 Profile of the Small Grating [5]

The pitch as determined from the stylus profilometer measurements is comparable to the pitch determined from the diffraction pattern of a simple diffraction experiment. The measured thickness of the smaller grating is, however, clearly different from the original film thickness (246 nm). In order to investigate this further, we asked Arun Vijayakumar from the University of Central Florida to analyze the samples using an optical profilometer. This technique combines optical interferometry with optical microscopy. A schematic drawing of the used instrument is shown in Fig. 2.4a. It is a non-destructive measurement technique, which means that there is no contact between the instrument and the surface of the sample. Light reflecting from the sample will interfere with light reflecting from a flat reference surface. Depending on the path

difference between both light beams, constructive or destructive interference will occur in the camera.

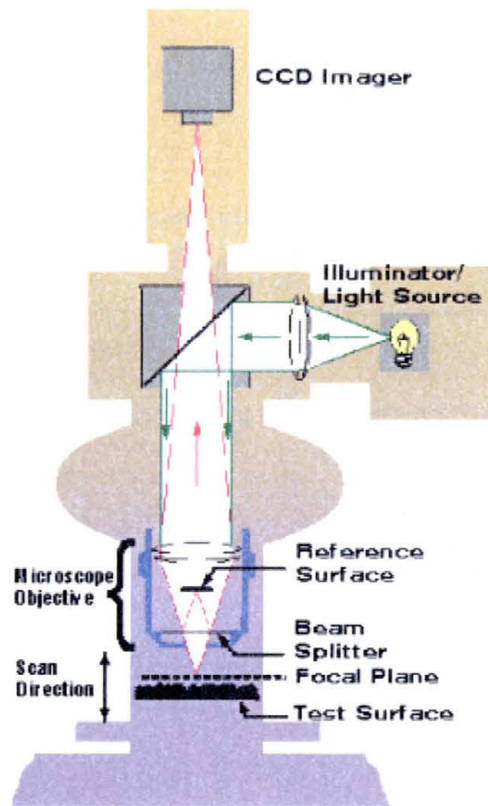


Figure 2.4 Optical Profilometer [13]

This set-up is extremely sensitive for height variations in the z-direction (perpendicular to the sample surface). It can resolve changes in the z-direction on the order of the sub-angstrom level. Figure 2.4 is a screen capture of a line scan. The surface profile of the grating is plotted on the y-axis as a function of the position. The line scan was done perpendicular to the strips of the grating.

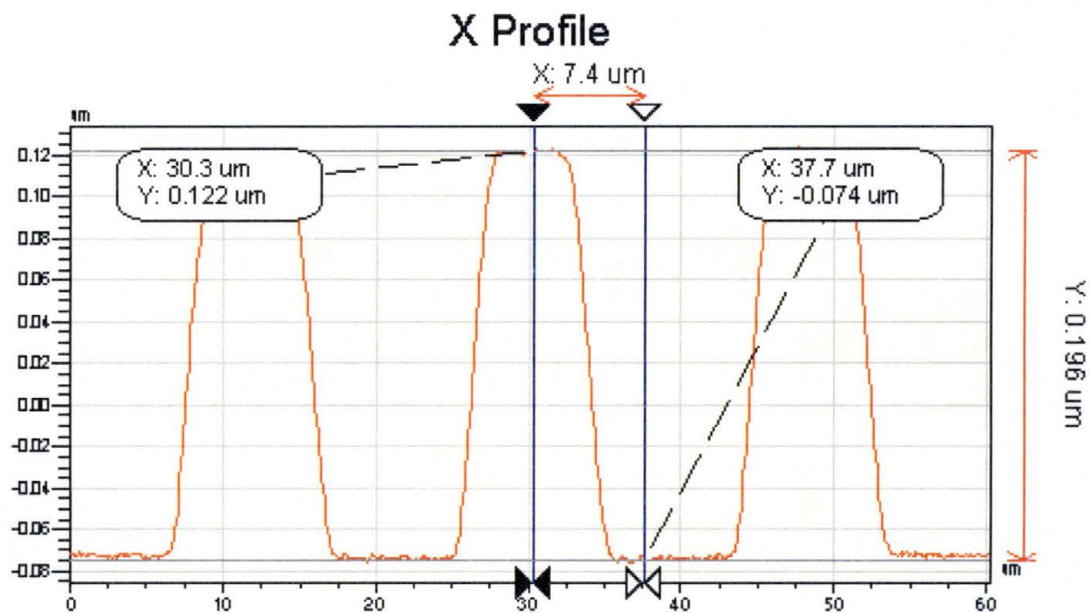


Figure 2.5 Thickness Versus X-Direction Raw Data. Optical Profilometer Scan on Sample 102501L01

Two dimensional profiles of the three gratings in sample 20250101 are given in Fig. 2.5, 2.6, and 2.7.

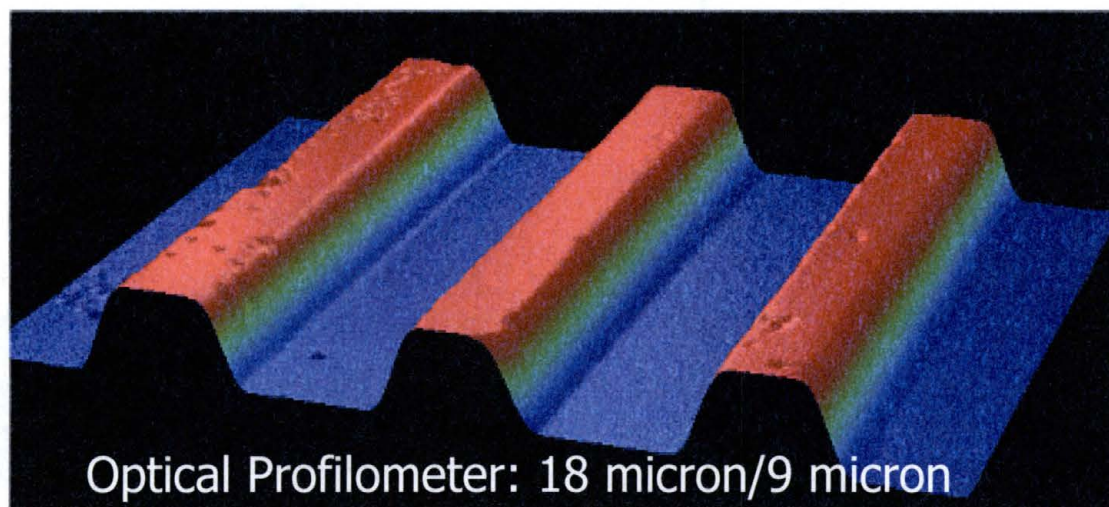


Figure 2.6 Profile of the Large Grating.

This measurement technique enables us to see the actual profile of the gratings. By looking at this image, we can see that the sides of the grating lines are not vertical and that the film and the substrate are rough.

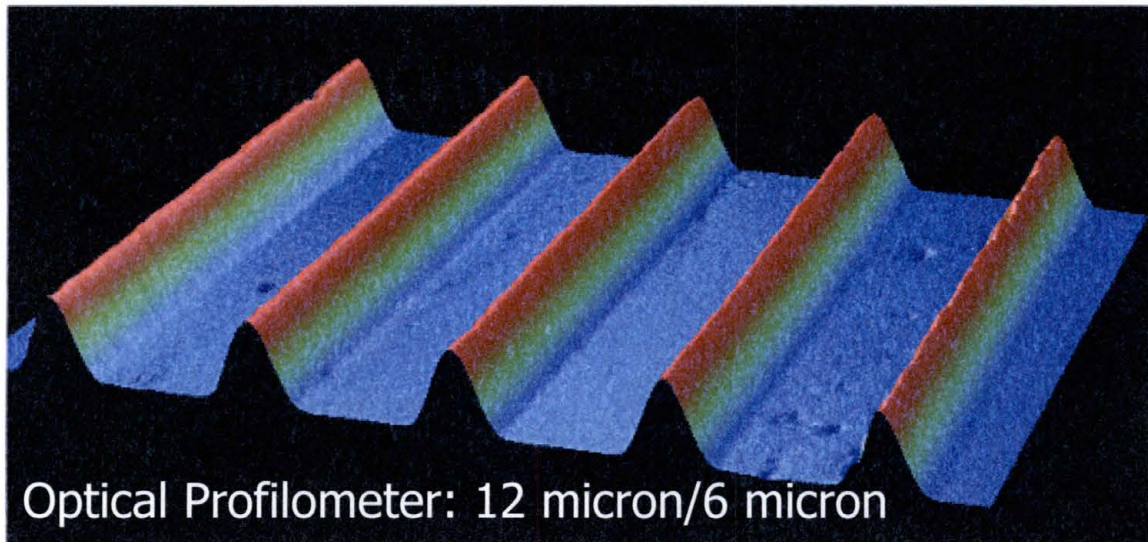


Figure 2.7 Profile of the Medium Grating.

For the medium grating, we see that the sides also have an angle, and we also see a roughness in the film and the substrate.

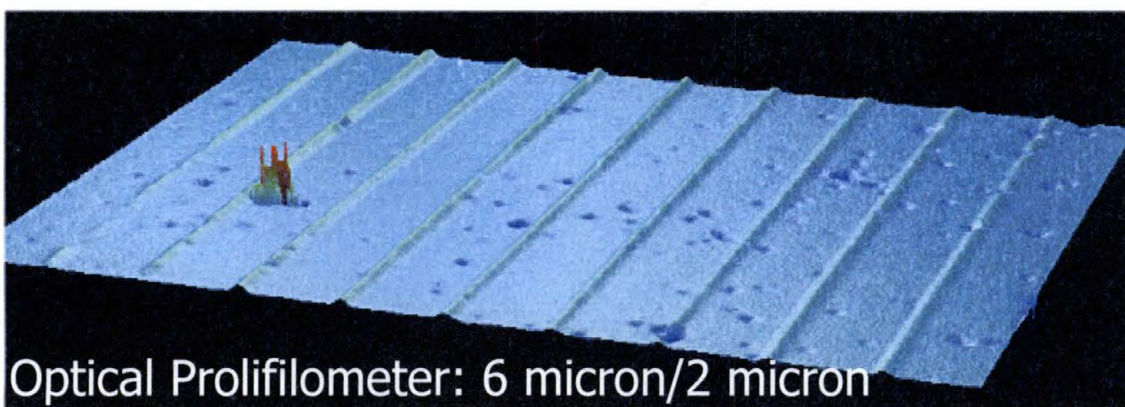


Figure 2.8 Profile of the Small Grating.

For the small grating, we see that there is not much film left on the substrate, and that the substrate is very rough. We believe that under-etching caused by the poor adhesion of the photoresist to the NiFe film causes the inclined side walls and causes the smaller grating to have a much thinner film thickness. The data from the optical profilometer is in agreement with the data that was taken with the stylus profilometer. The thickness as measured by the optical profilometer is approximately 200 nm.

CHAPTER 3

MAGNETO-OPTICAL KERR EFFECT

In this chapter, the interaction of an electro-magnetic wave (EM-wave) with a magnetic material is described. It is assumed that the material is magnetized along the x-direction. Figure 3.1 shows the above-considered configuration.

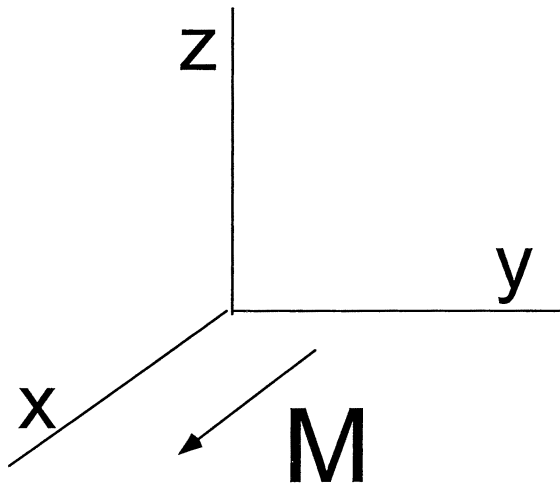


Figure 3.1 Direction of Magnetization

When light interacts with a material, electrons experience a force because of the electric field of the electro-magnetic wave (EM-wave). The effect of the magnetic field of the EM-wave, at these high frequencies

(10^{14} Hz), is marginal and normally neglected. The electric force will make the electrons oscillate parallel to the electric field component (E-component) of the EM-wave. This motion can be considered to be an AC (alternating current) current. The oscillating charge will create an electromagnetic wave that is linearly polarized along the same direction as the incident EM-wave.

If we assume that there is a magnetic molecular field in a ferromagnetic material, these moving charges will be subject to a magnetic force perpendicular to this oscillating motion and perpendicular to the magnetic field. So the charge will also have a small oscillating component perpendicular to the x-direction. This component is responsible for the Magneto-Optical Kerr effect. In this chapter we will derive a classical theory for the Kerr effect.

As mentioned above, the electric field of an EM-wave will polarize the atoms and exert a force on the conduction electrons. In this chapter we will only consider the latter. The oscillating conduction electrons will collide with lattice imperfections or crystal boundaries in the material. Every time an electron collides with an imperfections or crystal boundary it will lose all of its drift velocity. This means that just after the collision the direction of the velocity will be at random. The force caused by the electric field of the EM-wave will then immediately start accelerating the electron in a direction parallel to it. If we assume that the average time between two collisions is τ , then the average terminal velocity depends on

τ and the acceleration of the electron. The equation that we use for this is:

$$v_{term} = at + v_0 \quad (3.1)$$

where a is the acceleration, t is the time, and v_0 is the initial velocity.

After the collisions, the average initial velocity is 0 so the equation can be simplified to:

$$v_{term} = at = a\tau \quad (3.2)$$

Solving this equation for a , we get:

$$a = \frac{v_{term}}{\tau} \quad (3.3)$$

If we plug equation 3.3 into Newton's Law, we will get for the y direction

$$F_y = ma_y = \frac{mv_y}{\tau} \quad (3.4)$$

This F_y is also equal to the sum of the electric force and the magnetic force. The magnetic force is caused by an externally applied magnetic field, or in the case of a ferromagnetic material caused by an effective field the so-called molecular field [14]. The molecular field can be considered to be proportional to the magnetization. Our equation for the total force in the y direction is now (realize that $F = q \mathbf{v} \times \mathbf{B}$)

$$F_y = -eE_y - \frac{e}{c}v_z B_x \quad (3.5a)$$

where e , E_y , c , and B_x , are the charge of the electron, the electrical field in the y direction, the speed of light, and the effective magnetic field in

the thin film in the x direction, respectively. Similarly we find for the z-direction and the x-direction (realize that $F = q \mathbf{v} \times \mathbf{B}$):

$$F_z = -eE_z + \frac{e}{c} v_y B_x \quad (3.5b)$$

$$F_x = -eE_x \quad (3.5c)$$

From this point on we will use the force equation in the y direction, but the same method is used in the derivation for the force in the z direction. The first step in the derivation is to combine equation 3.4 and 3.5a and to multiply both sides by:

$$\frac{-ne}{m} \quad (3.6)$$

When we do this, we get:

$$-n \cdot e \cdot v_y = \frac{\tau \cdot n \cdot e^2}{m} \cdot E_y + \frac{\tau \cdot n \cdot e^2}{m \cdot c} \cdot v_z \cdot B_x \quad (3.7)$$

where n is the number of charge carriers per unit volume, τ is the relaxation time (average time between collisions), and m is the mass of an electron. We also know that the current density \mathbf{j} can be written as

$$\mathbf{j} = -n \cdot e \cdot \mathbf{v} \Rightarrow j_y = -n \cdot e \cdot v_y \quad (3.8)$$

If we substitute equation 3.8 into equation 3.7, we get:

$$j_y = \frac{\tau \cdot n \cdot e^2}{m} \cdot E_y - j_z \cdot \frac{\tau \cdot e}{m \cdot c} \cdot B_x \quad (3.9a)$$

When we apply this derivation to the force equation in the z direction, we get:

$$j_z = \frac{\tau \cdot n \cdot e^2}{m} \cdot E_z + j_y \cdot \frac{\tau \cdot e}{m \cdot c} \cdot B_x \quad (3.9b)$$

$$j_x = \frac{\tau \cdot n \cdot e^2}{m} \cdot E_x \quad (3.9c)$$

We can now substitute equation 9b into 9a. If we do this we get

$$j_y = \frac{\tau \cdot n \cdot e^2}{m} \cdot E_y - \frac{\tau \cdot e}{m \cdot c} \cdot B_x \cdot \left(\frac{\tau \cdot n \cdot e^2}{m} \cdot E_z + j_y \cdot \frac{\tau \cdot e}{m \cdot c} \cdot B_x \right) \quad (3.10)$$

The next steps are to distribute and rearrange terms so that the outcome looks like

$$j_y + \frac{e^2 \cdot \tau^2}{m^2 \cdot c^2} \cdot B_x^2 \cdot j_y = \frac{n \cdot e^2 \cdot \tau}{m} \cdot E_y - \frac{n \cdot e^3 \cdot \tau^2}{m^2 \cdot c} B_x \cdot E_z \quad (3.11)$$

This equation can be simplified further by pulling the j_y terms from the left side of the equation.

We now have an equation that looks like this:

$$j_y \left(1 + \frac{e^2 \cdot \tau^2}{m^2 \cdot c^2} \cdot B_x^2 \right) = \frac{n \cdot e^2 \cdot \tau}{m} \cdot E_y - \frac{n \cdot e^3 \cdot \tau^2}{m^2 \cdot c} B_x \cdot E_z \quad (3.12)$$

The next two equations will be used to substitute in the equation to simplify it further.

$$\omega_c = \frac{e}{m \cdot c} \cdot B_x \quad (3.13)$$

$$\sigma_0 = \frac{n \cdot e^2 \cdot \tau}{m} \quad (3.14)$$

where ω_c is called the Larmor frequency, which is proportional to the effective magnetization field, and σ_0 is the traditional conductivity.

The equation now looks like:

$$j_y \left(1 + (\omega_c \cdot \tau)^2\right) = \sigma_0 \cdot E_y - \frac{\sigma_0 \cdot e \cdot \tau}{m \cdot c} \cdot B_x \cdot E_z \quad (3.15)$$

The next step is to solve the equation for the current density.

$$j_y = \frac{\sigma_0}{\left(1 + (\omega_c \cdot \tau)^2\right)} \cdot E_y - \frac{\sigma_0 \cdot \omega_c \cdot \tau}{\left(1 + (\omega_c \cdot \tau)^2\right)} \cdot E_z \quad (3.16a)$$

We can also plug equation 3.9a into 3.9b and solve for the current density in the z-direction. This will give:

$$j_z = \frac{\sigma_0}{\left(1 + (\omega_c \cdot \tau)^2\right)} \cdot E_z + \frac{\sigma_0 \cdot \omega_c \cdot \tau}{\left(1 + (\omega_c \cdot \tau)^2\right)} \cdot E_y \quad (3.16b)$$

If we plug in the E component that is parallel to the x-direction into the Lorentz equation, the force due to the magnetic field, which is in the x-direction, is:

$$F_B = e(v_x \times B_x) = e \cdot v_x \cdot B_x \cdot \sin \phi = e \cdot v_x \cdot B_x \cdot \sin 0 = 0 \quad (3.17)$$

where e is the charge of an electron, v_x is the velocity in the x-direction, B_x is the magnetic field in the x-direction and ϕ is the angle between B_x and v_x . Since the angle is zero, the force due to the magnetic field is also zero. If we go through the derivation for the current density in the x-direction, we will only get a contribution from the E-field in the x-direction and the equation for the current density will be:

$$j_x = \sigma_0 \cdot E_x \quad (3.18)$$

We can now express equations 16, 16a, and 18 in matrix form to show the conductivity tensor:

$$\begin{pmatrix} j_x \\ j_y \\ j_z \end{pmatrix} = \hat{\sigma} \begin{pmatrix} E_x \\ E_y \\ E_z \end{pmatrix} \quad \text{Where} \quad \hat{\sigma} = \begin{pmatrix} \sigma_0 & 0 & 0 \\ 0 & \sigma_{yy} & \sigma_{yz} \\ 0 & \sigma_{zy} & \sigma_{zz} \end{pmatrix} \quad (3.19)$$

with:

$$\sigma_{zz} = \sigma_{yy} = \frac{\sigma_0}{1 + (\omega_c \cdot \tau)^2} \quad (3.20)$$

$$\sigma_{yz} = -\frac{\sigma_0 \cdot \omega_c \cdot \tau}{1 + (\omega_c \cdot \tau)^2} = -\sigma_{zy} \quad (3.21)$$

If the incident light is polarized parallel to the magnetization, in our case in the x-direction, there will only be a current induced parallel to the x-axis. Since this current is parallel to the x-axis the reflected EM-wave will only have a component parallel to the x-axis also. If we refer to equations 3.14 and 3.18 we see that the current and σ_0 are both independent of ω_c and therefore independent of the magnetization. This means that for a current in the x-direction, there will not be any Magneto-Optical effects.

If the incident light is polarized in the y-direction, then a current will be induced in both the y-direction and in the z-direction. This means that the reflected light is no longer polarized parallel in the y-direction, but it will also have a component parallel to the z-direction. Since $\sigma_{yy}, \sigma_{zz}, \sigma_{yz},$ and σ_{zy} all depend on ω_c , and therefore the magnetization, the polarization of the reflected light depends on the magnetization of the material. This effect is called the Magneto-Optical Kerr Effect.

The diagonal components of the conductivity tensor are normally considered to be independent of the magnetization, so that the only

components that depend on the magnetization are the off-diagonal terms, σ_{yz} and σ_{zy} , of the conductivity tensor. Looking at equation 3.21, we can see that they only depend to the first order on ω_c . This means that they are odd functions of the magnetization. Since they are odd functions of the M , then they are also a good indicator for the measurement of the magnetization of the material being studied. According to equation 3.21 the diagonal components also depend on ω_c . According to equation 3.20 they depend on the inverse square of ω_c , which is proportional to M^{-2} . This means that they are an even function of the magnetization. These so called non-linear effects are normally neglected. In chapter 5, however, it is shown that non-linear effects can significantly contribute to the magneto-optical properties.

According to the equations 3.19, the linear and non-linear effects are only observed if the incident light has a component that is polarized along the y - and/or z -direction. If the incident light is strictly polarized along the x -direction, i.e. along the magnetization, no MO Kerr effect is observed. This is because σ_0 is independent of ω_c or M . So by choosing the polarization of the incident light along a certain direction, it is possible to make the MO measurement technique sensitive for only certain components of the magnetization vector. Figure 3.2 shows a measurement configuration that is insensitive to components of the magnetization perpendicular to the plane of incidence.

We now have an idea of how free electrons contribute to the optical properties. There are also bound electrons that contribute to the optical properties. Since the electrons are bound, we will talk about them in terms of the displacement instead of the current density. The Displacement vector is related to the E-field by the equation:

$$\vec{D} = \hat{\epsilon}_0 \cdot \vec{E} \quad (3.22)$$

where $\hat{\epsilon}_0$ is the dielectric tensor, D is the displacement vector, and E is the electric field. The dielectric tensor is also a matrix. It is expected that also the components of ϵ_0 matrix will depend on the molecular field.

We can see the effect of both of the dielectric tensor and the conductivity tensor by combining them to form the effective dielectric tensor. The effective dielectric tensor can be written as:

$$\tilde{\epsilon} = \tilde{\epsilon}_0 + \frac{4 \cdot \pi \cdot \tilde{\sigma}}{i \cdot \omega} \quad (3.23)$$

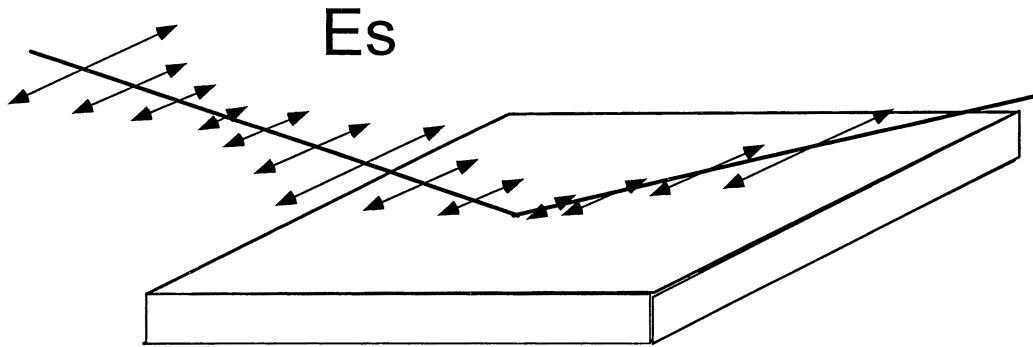


Figure 3.2 Measurement configuration that is insensitive to components of the magnetization perpendicular to the plane of incidence

CHAPTER4

MAGNETO-OPTICAL KERR TRACER AND KERR MICROSCOPE

4.1 The Original Kerr Tracer Measurement Technique

The ellipsometer used to determine the hysteresis curves for the nickel-iron gratings is a Polarization Modulated Ellipsometer (PME) as first proposed by Jaspersen et al. [1]. In these ellipsometers, the polarization of the incident beam is modulated by a photo-elastic modulator (PEM) while the intensity of the reflected light is measured with a photodiode or a photomultiplier tube. It is possible to determine the ellipsometric quantities Δ and Ψ [2], from the dc-component, 1ω component, and 2ω component of the detector signal. More details on the measurement technique can be found in [1,2]. Polarization Modulated Ellipsometry (PME) was first used by Sato et al. to study the magnetic properties of magnetic thin films [6]. For the Polar configuration (magnetic field perpendicular to the plane of the film) the magneto-optical Kerr rotation (θ) and the magneto-optical Kerr ellipticity (η) are linearly proportional to the 2ω and 1ω detector signal. In other words [7]:

$$\begin{aligned}
I_{tot} &= I_{DC} + I_{\omega} + I_{2\omega} \\
I_{\omega} &= A * \eta_k \\
I_{2\omega} &= B_t \theta_k
\end{aligned}
\tag{4.1}$$

Where I_{tot} is the intensity measured by the detector, I_{DC} is the DC detector signal, I_{ω} is the one- ω detector signal, and $I_{2\omega}$ is the two- ω detector signal.

Recently others have used PME to measure the in-plane component of the magnetization. Measurements are done in the longitudinal (magnetic field parallel to the film plane and parallel to the plane of incidence) or transverse mode (magnetic field parallel to the film plane and perpendicular to the plane of incidence) [8]. For transverse and longitudinal measurements, the angle of incidence is unequal to zero. It is normally assumed that the magnetization is parallel to the plane of the film and that the samples are isotropic and have no in-plane anisotropy axis.

4.2 The Magneto-Optical Kerr Ellipsometer Setup

The experimental setup consists of six major components. They are the Helium-Neon (HeNe) laser, a polarizer, a photo-elastic modulator, the sample, an analyzer, and a photo-multiplier tube. Figure 4.1 shows a drawing of the ellipsometer.

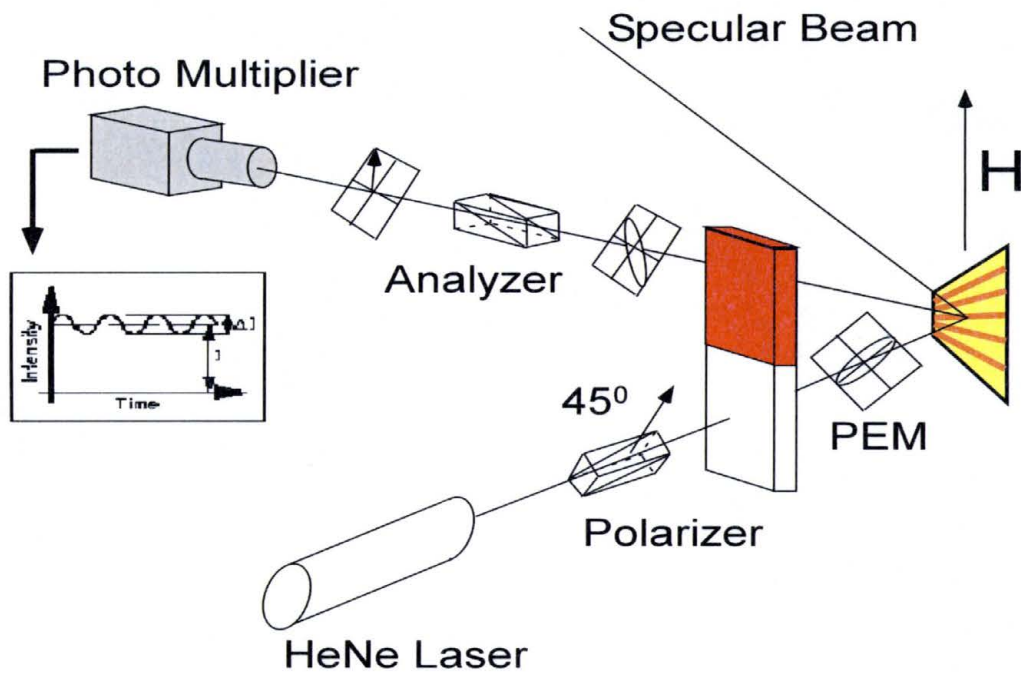


Figure 4.1 The Magneto-Optical Kerr Ellipsometer Setup

The laser (type and specifications) used in this experiment had a wavelength was 632.8 nm, and the beam spot size was 280 μm in diameter. The polarizer and the PEM were fixed together and the PEM was kept at a -45° with respect to the polarizer. The sample consisted of a NiFe film on top of a one inch p-type Si wafer. The samples were prepared by magnetron sputtering. More details on the sputtering process can be found in [3]. Gratings with a size of 1 X 1 mm^2 were etched in the NiFe film using the laser beam writer and a diluted aluminum etchant. More details on the sample can be found in chapter 2 and [5]. The grating causes diffraction of the reflected beam. Measurements can be done by selecting one of the diffracted beams.

Before starting a measurement the analyzer is adjusted to minimize the 1ω or 2ω detector-signal . The photo-multiplier tube is placed after the analyzer and is used to translate the light signal into an electronic signal that is then sent to the lock-in amplifier.

The measurement system is controlled by a user interface created by a former student named Harsha Abewickrema. The program is designed to control the magnet's power supply as well as read the input from the multi-meter, the lock-in amplifier, and the readings from the magnetic field and create a hysteresis curve. Each component is connected to a PC by a GPIB cable and interface board. The PEM is connected to the lock-in amplifier. The detector signal is also connected to this lock-in amplifier. A lock-in amplifier is used so that the resulting signal could be compared to the reference frequency. It acts like a narrow bandwidth amplifier that will reject noise and other signals. Figure 4.2 shows a schematic diagram of the measurement system.

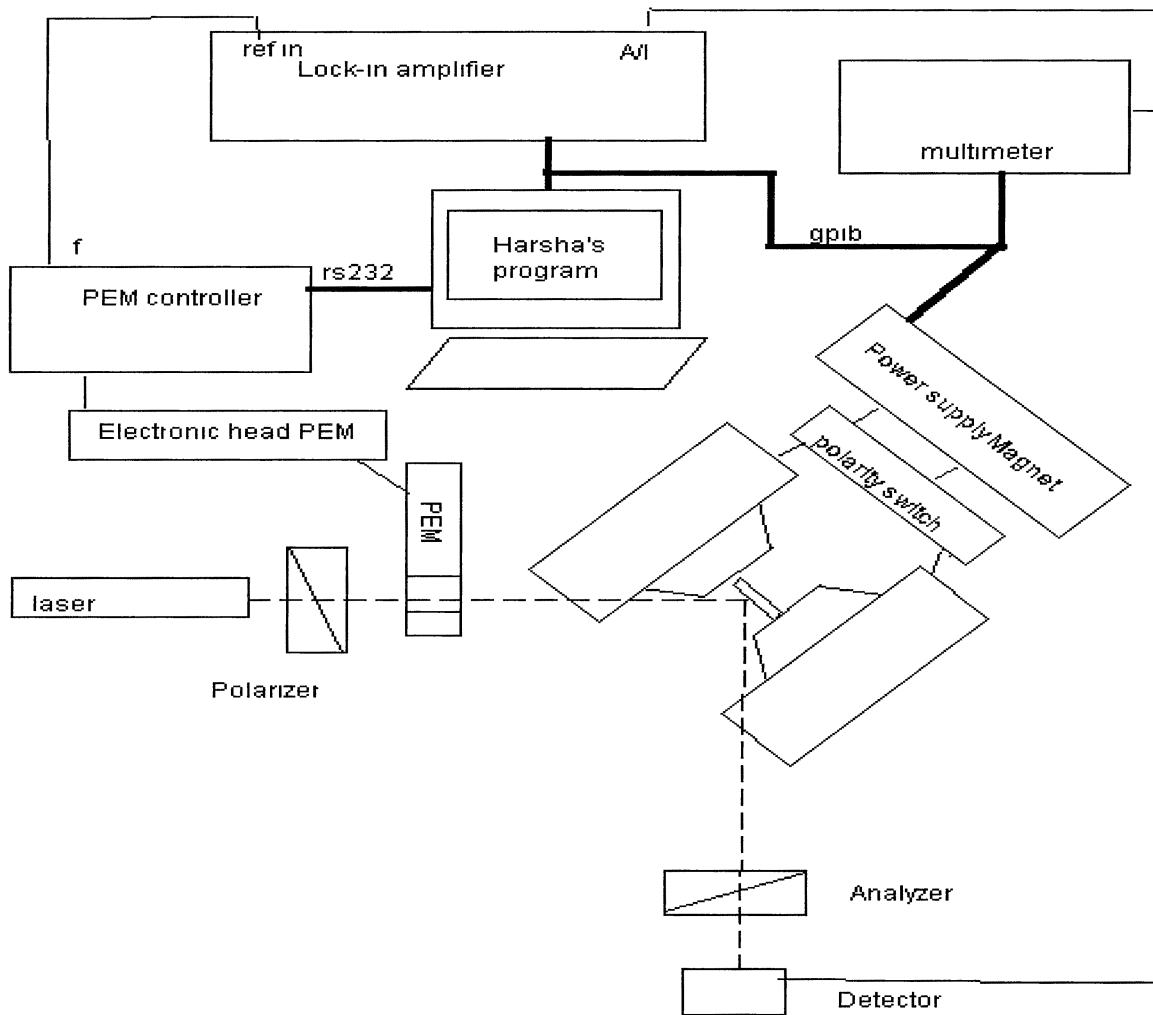


Figure 4.2: Block diagram of the Kerr setup

When the analyzer is set to 0 degrees with respect to the plane of incidence ($\phi=0$), the detected intensity can be written as [7]:

$$I = I_0(1 + 2(\theta_k \cos \delta - \eta_k \sin \delta)) \quad (4.2)$$

In the derivation of equation (4.2) we assumed that θ_k is small and that $\sin(2\theta_k)$ can be approximated by $2\theta_k$. Furthermore, I_0 is related to the source intensity and reflectivity of the sample [11], θ_k and η_k are the Kerr

rotation and the Kerr ellipticity signals, respectively, and δ is the retardation angle which is a function of the time and is given by

$$\delta = \delta_0 \sin \omega t \quad (4.3)$$

where ω is $2\pi f$ ($f=50$ Khz). If equation 4.3 is plugged into equation 4.2 and then equation 4.2 is normalized, then the following equation is the result:

$$\frac{I}{I_0} = (1 + 4J_2(\delta_0)\theta_k \sin 2\omega t - 4J_1(\delta_0)\eta_k \sin \omega t + \dots), \quad (4.4)$$

in which J_n is the n^{th} Bessel function [11]. This means that the η_k is detected when measuring the one- ω signal of the detector and θ_k is detected when measuring the 2ω signal of the detector.

4.3 The Kerr Microscope Setup

The two most common types of Kerr microscopes are shown in figure 4.3. The image on the left is a low-resolution microscope that has a resolution of approximately $2 \mu\text{m}$, and it is used to obtain domain patterns of larger samples [9]. The image on the right shows a high resolution Kerr microscope. This type of setup can resolve domains as narrow as $0.15 \mu\text{m}$ with a total resolution to be $0.3 \mu\text{m}$ [9].

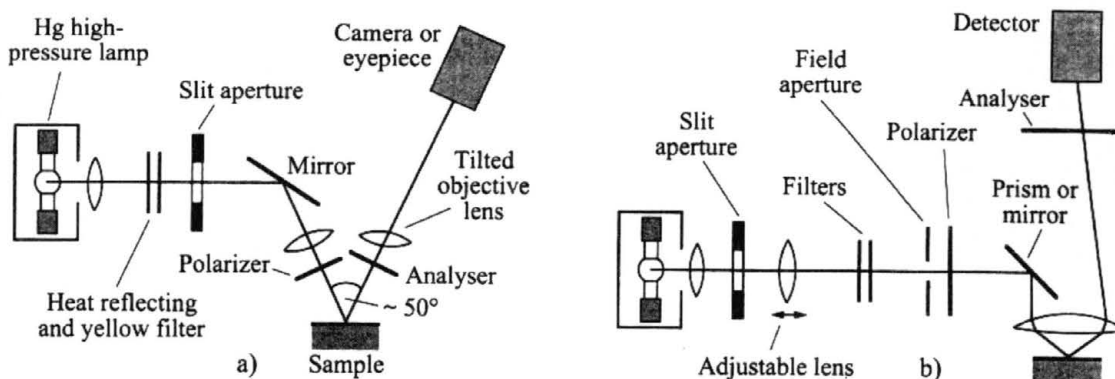


Figure 4.3 Two Types of Kerr Microscopes, a) low resolution with high sensitivity, b) High resolution distortion free Kerr microscope [9]

The type of Kerr Microscope that was used in this experiment is a modification of Figure 4.3b. The measurement system used in this part of the experiment was designed and constructed at the University of Twente by Casper Doppen [12]. It consists of several components. The major components are the magnet, sample stage, objective, a light source (arc lamp, $\lambda \approx 520$ nm), filters, polarizer, a semitransparent mirror, a regular mirror, an analyzer, and a CCD camera. Figure 4.4 is a schematic of the full setup. The setup can be used to measure the two in-plane components of the magnetization. Depending on the orientation of the polarizer two different components of the magnetization, i.e. parallel or perpendicular to the plane of incidence, can be detected. More details can be found in chapter 3 and [9].

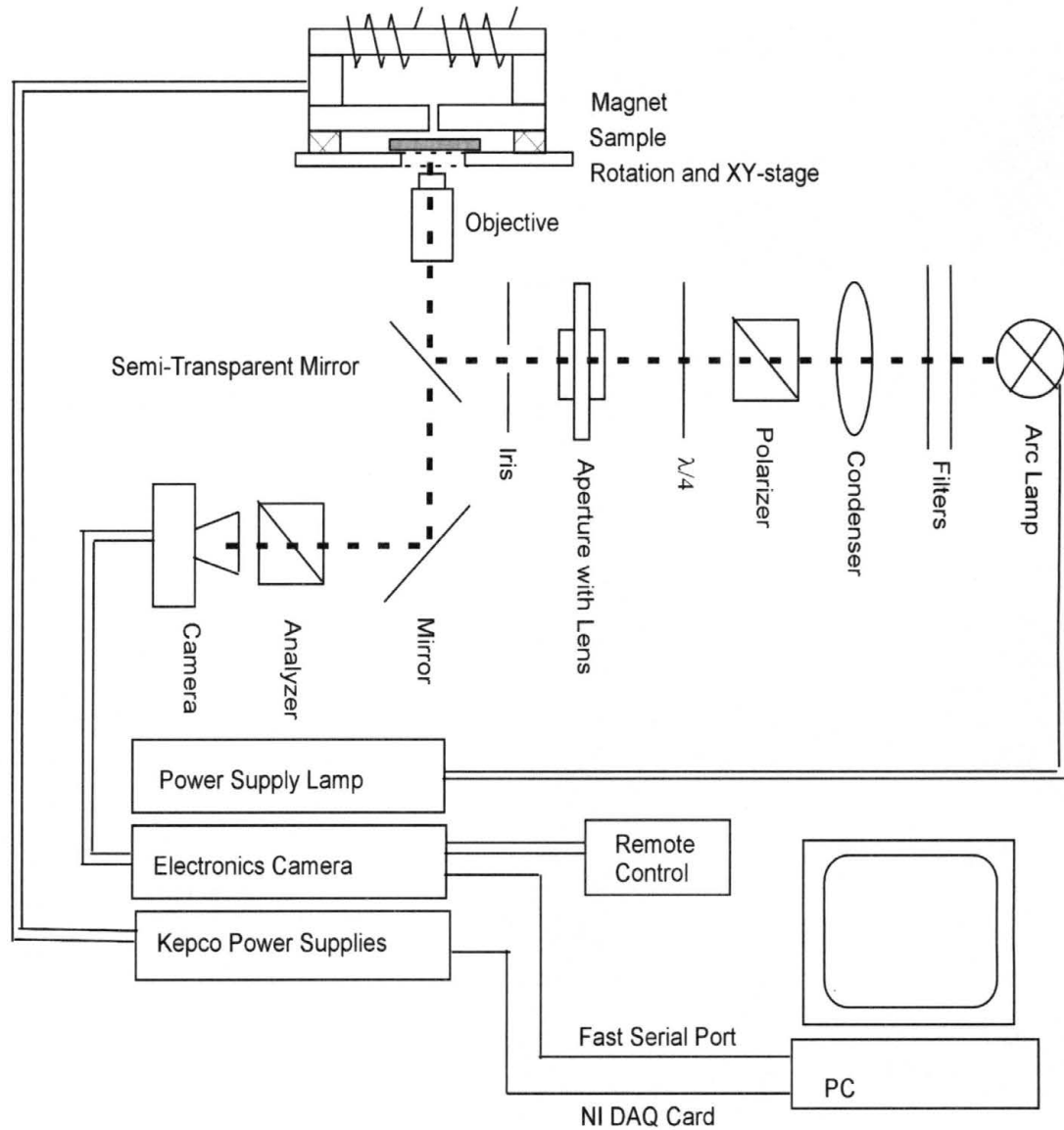


Figure 4.4 Block Diagram of the Kerr Microscope Setup

To produce the images for domain analysis, a series of steps had to be performed. The first step was to take an image where the sample region was completely saturated (all of the domains are in one direction). This picture was used as a reference image. The next step involved

taking another image when the applied field is set such that there is a change in direction of some domains in the film. This picture and the reference picture were then compared to each other using a program that subtracts both images. In this way the contrast according to the roughness of the sample will cancel out and only the magnetic contrast will remain in the data-processed picture. Figure 4.5 shows the final pictures after the subtraction has been done. Figure 4.5 a shows the domain pattern sensing the horizontal component of the magnetization of sample 10250101, and Fig. 4.5 b shows the domain pattern sensing the vertical component of the magnetization at exactly the same location on the sample.

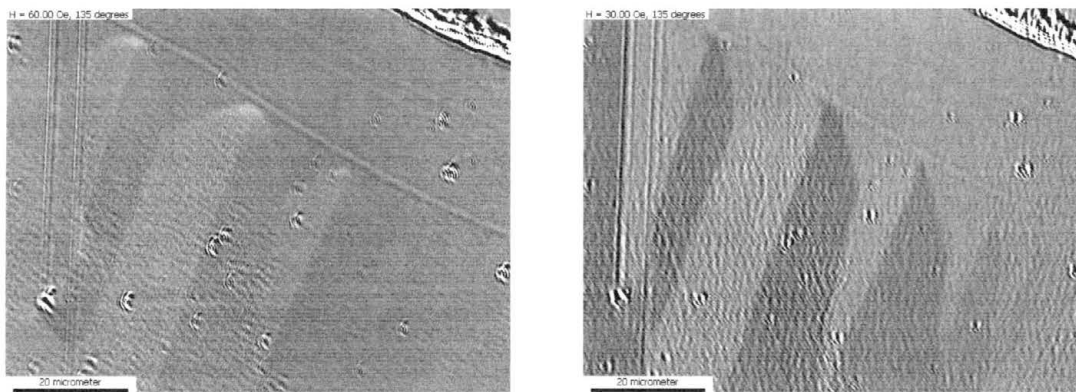


Figure 4.5: Domain pattern of sample 10250101: (a) horizontal component of the magnetization; (b) vertical component of the magnetization

CHAPTER 5

MAGNETO-OPTICAL KERR TRACER SET-UP TESTING AND PREPARATION

5.1 Set-up Testing

To get a better understanding for the origin of the measurement anomalies of Figure 1.2, two main aspects of the set-up were tested. At first I checked the dependence of the retardation amplitude of the modulator to verify the theory discussed in chapter four. Second, I determined the effects of the PEM angle on the measured hysteresis curve. The PEM is composed of a fused silica bar that is connected to a quartz piezoelectric transducer. The transducer controls the length of the silica bar. When the silica is stressed in, for example, the x-direction, the speed at which light linearly polarized in the x-direction travels through the crystal changes. The length extension and contraction causes a birefringence of the light, which means that light linearly polarized at different angles travel through the silica bar at different speeds[12]. The amplitude at which the length of the silica bar is modulated determines the angle shift (retardation). The length of the bar is modulated at a frequency of 50 KHz. The PEM is fixed to a

polarizer plate that is held to a fixed angle of 45° with respect to the axis of the PEM. This causes the polarization of the light to be modulated between right and left elliptically polarized light. The sample that was used in this experiment was 10280104 NiFe 45%. Both of these tests were conducted on the large grating using the specular beam where the spot size of the incident beam was $280\ \mu\text{m}$, and thus smaller than the size of the grating.

5.1.1 Retardation Angle

The first test that was conducted consisted of measuring the dependence of Kerr ellipticity signal on the retardation angle of the modulator. It was done to verify that it corresponds to the theory given in chapter four. Looking at equation 4.4 we can see that the modulation depth dependence of the Kerr signals should have the form of a Bessel function. The Kerr ellipticity signal should be proportional to the first order Bessel function. This function is the odd function shown in Fig. 5.1.

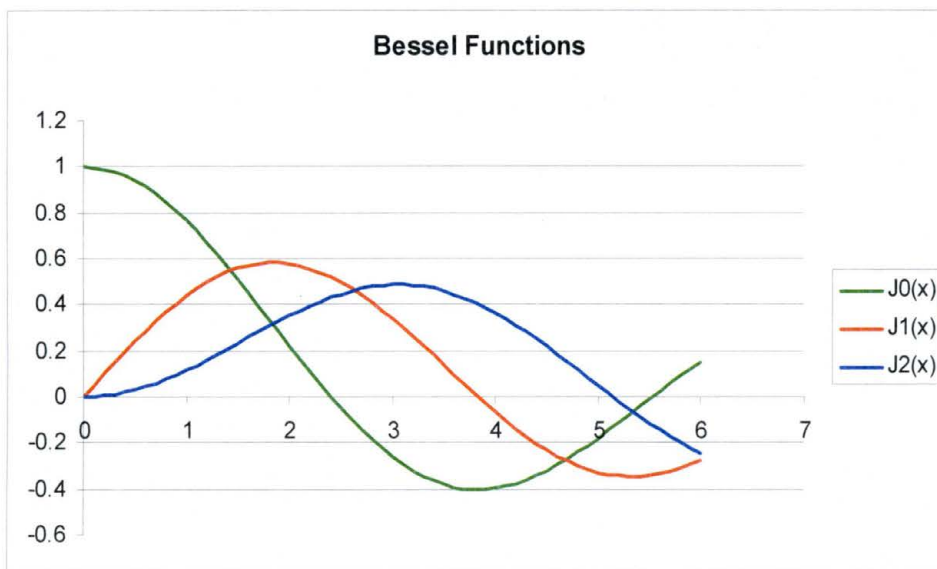


Figure 5.1 The First Three Bessel Functions

The set-up was tested by changing the depth of the retardation angle from 1.81 radians to 3.406 radians in increments of .1 radians. The shape of the measured hysteresis curve appeared to be independent of the retardation depth. We took the Kerr Ellipticity data for each one and found the difference between the maximum and minimum saturation values and graphed them versus the PEM retardation angle. Figure 5.2 shows this graph. There are two sets of points in this figure. The blue squares represent the first branch from one saturation level to the other, and the red triangles are for the reversal branch.

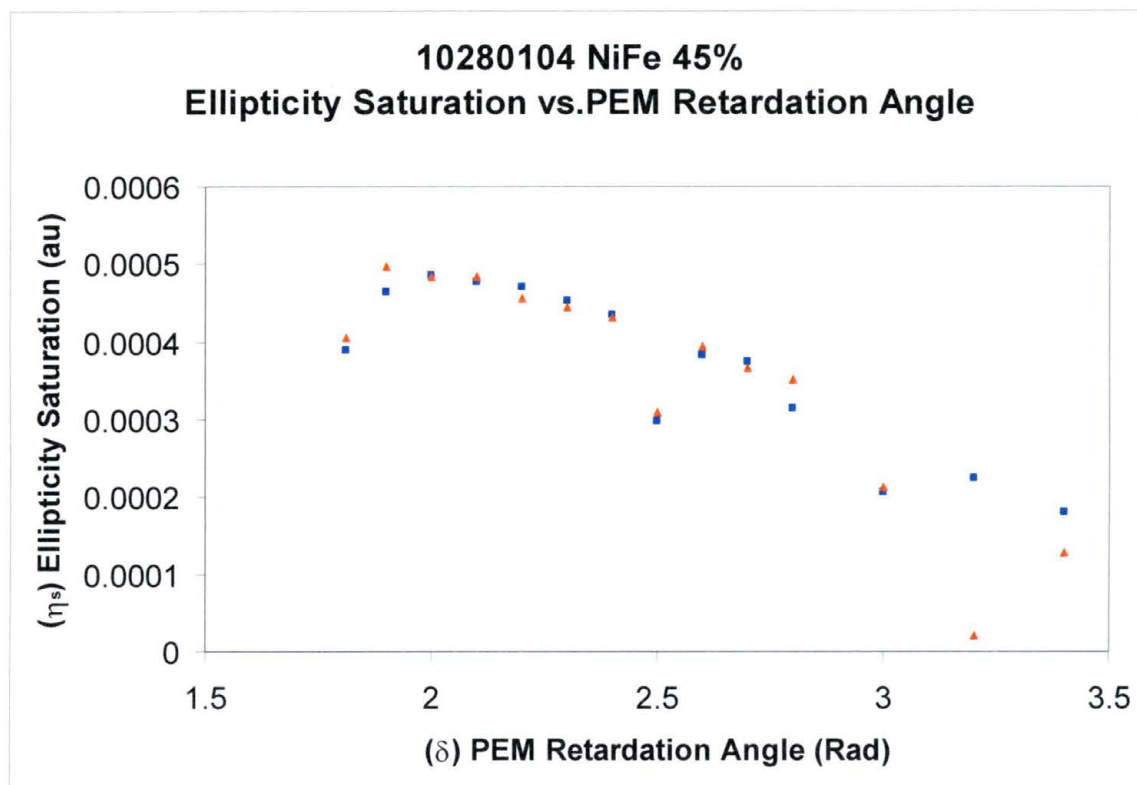


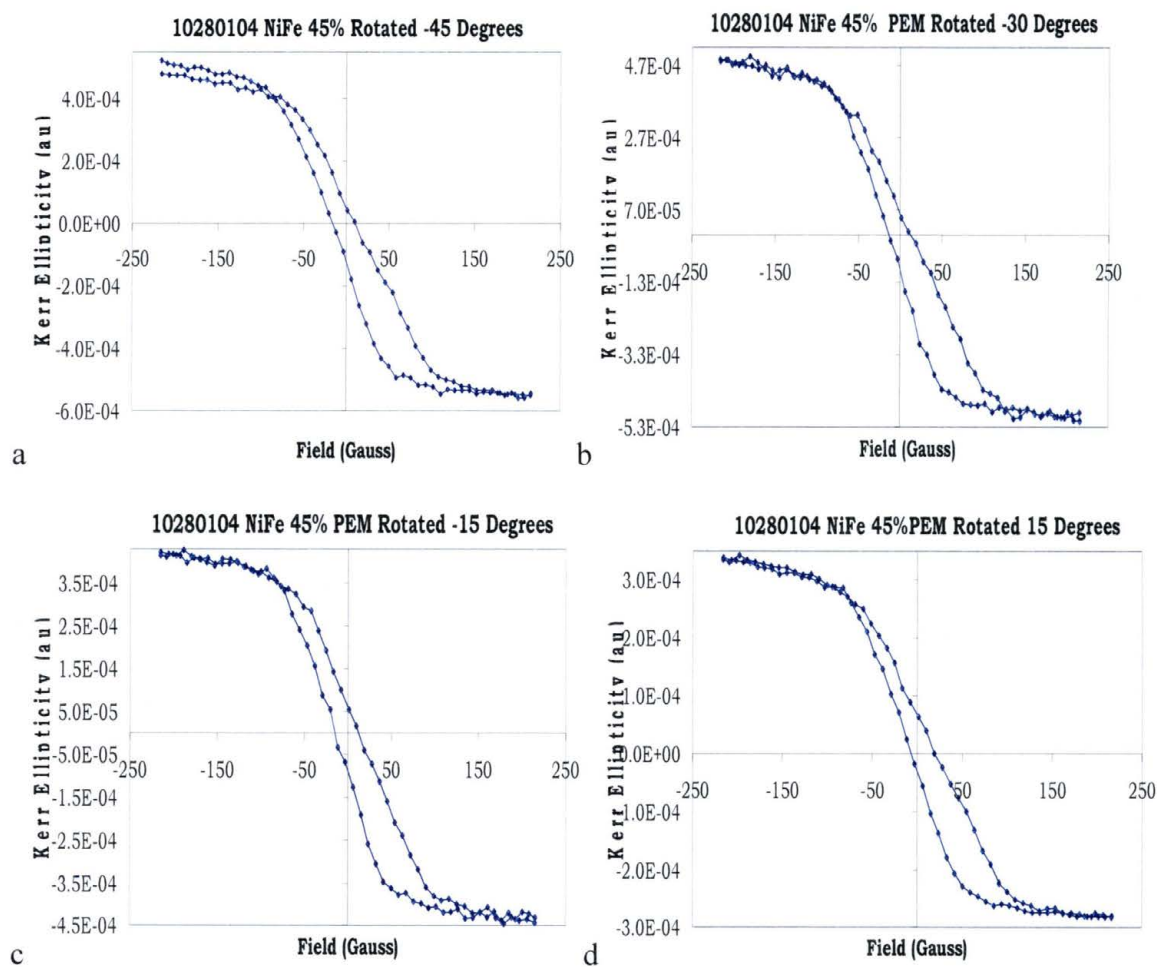
Figure 5.2 Ellipticity Saturation vs. PEM Retardation Angle

Comparing Figure 5.1 and Figure 5.2, there is a large similarity between the experimental data and the first order Bessel function. This means that the PEM retardation angle dependence follows the theory given in chapter four.

5.1.2 PEM Rotational Angle Dependence

The second test that we conducted was to determine the dependence of Kerr signals, if any, on the orientation of the PEM. So the Kerr ellipticity and Kerr rotation hysteresis curves were measured for different orientations of the PEM. The angle between the modulated axis of the PEM and the plane of incidence was varied from -45° to 45° in

steps of 15° . Figure 5.3 shows the Ellipticity hysteresis curves, i.e. MO Kerr ellipticity vs. applied magnetic field for different orientations of the PEM.



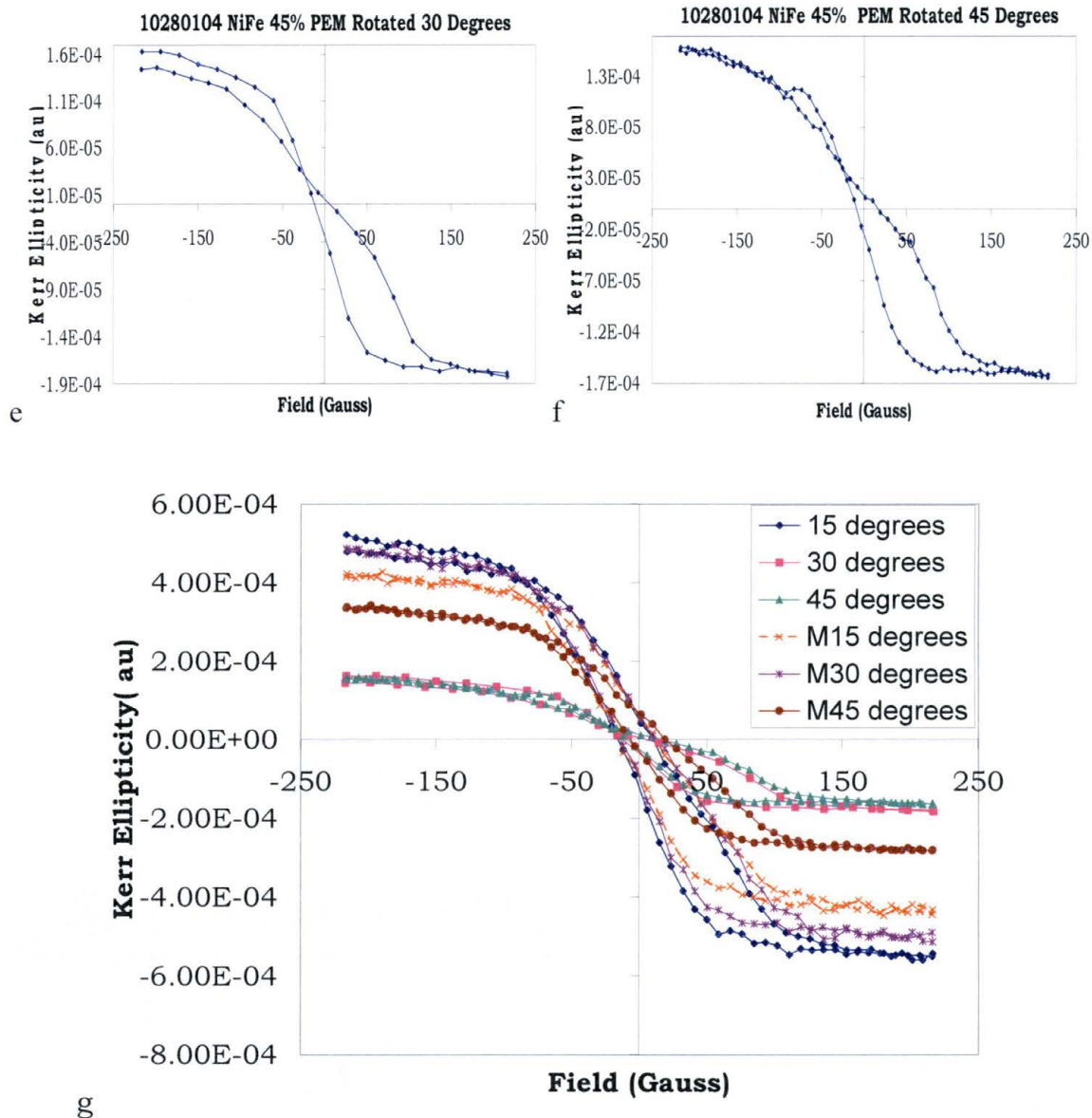
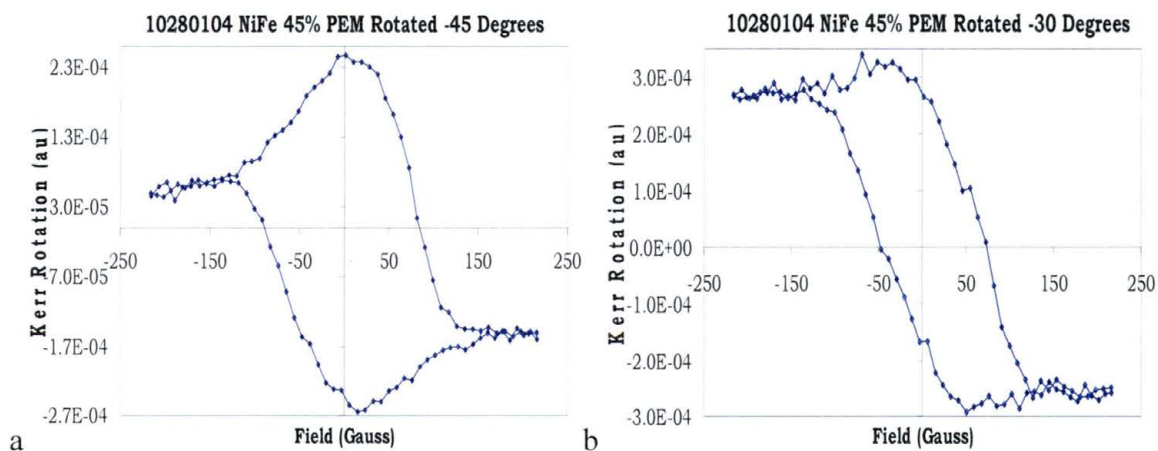


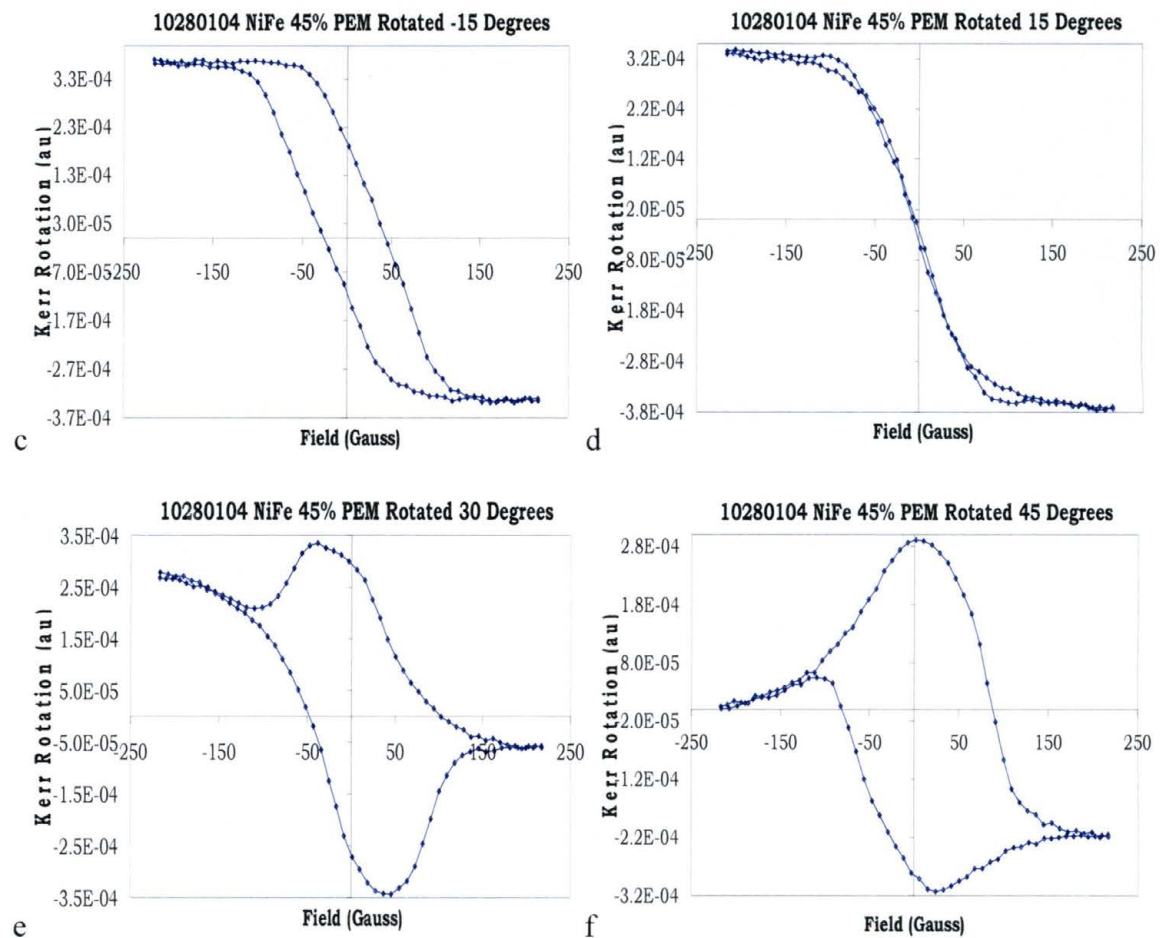
Figure 5.3 MO Kerr Ellipticity hysteresis curves for sample 10280104 for different orientations of the PEM: (a) -45 degrees; (b) -30 degrees; (c) -15 degrees; (d) 15 degrees; (e) 30 degrees; (f) 45 degrees; (g) comparison of all ellipticity curves to show differences in magnitude.

The first item to note when looking at this series is that these graphs are not all the same. The measured hysteresis curve depends on

the orientation of the PEM. We can conclude from this that the Kerr hysteresis curve no longer is a measure for the magnetic hysteresis curve. Another striking thing is that all of the Kerr curves are asymmetrical. Another item that can be seen is most pronounced in figure 5.3f. We are seeing what appears to be a rise and then fall on the final sweep. This term is called a negative susceptibility, which is a characteristic of a superconductor, or a diamagnetic material, and not a ferromagnetic material. We are not sure of what exactly is happening here.

Figure 5.4 shows the measured Kerr rotation vs. applied magnetic field.





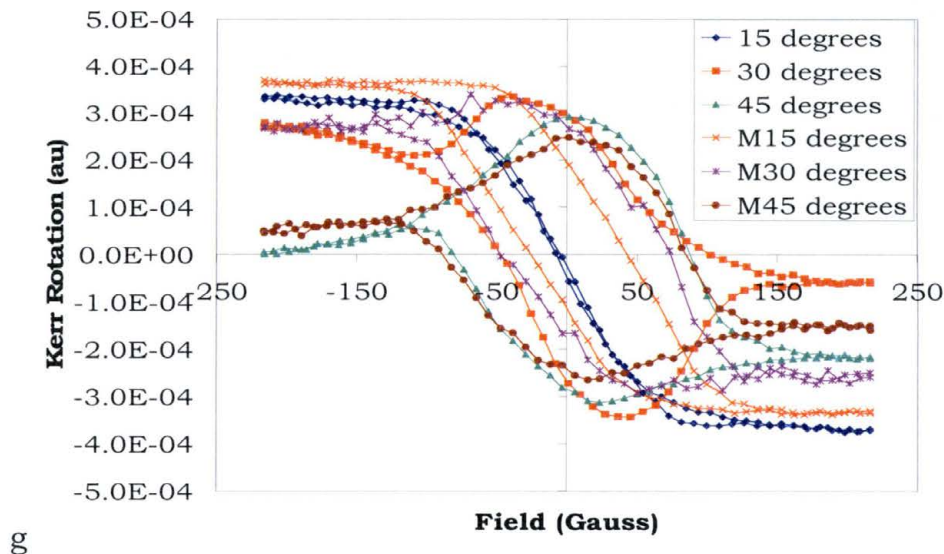


Figure 5.4 MO Kerr rotation hysteresis curves for sample 10280104 for different orientations of the PEM: (a) -45 degrees; (b) -30 degrees; (c) -15 degrees; (d) 15 degrees; (e) 30 degrees; (f) 45 degrees; (g) comparison of all rotation curves to show differences in magnitude.

The asymmetric effects that we saw with the Kerr Ellipticity graphs are still present in these Kerr Rotation graphs. We are seeing them with less magnitude, however. The negative susceptibility effect is very clearly seen in, for example, Fig. 5.4f.

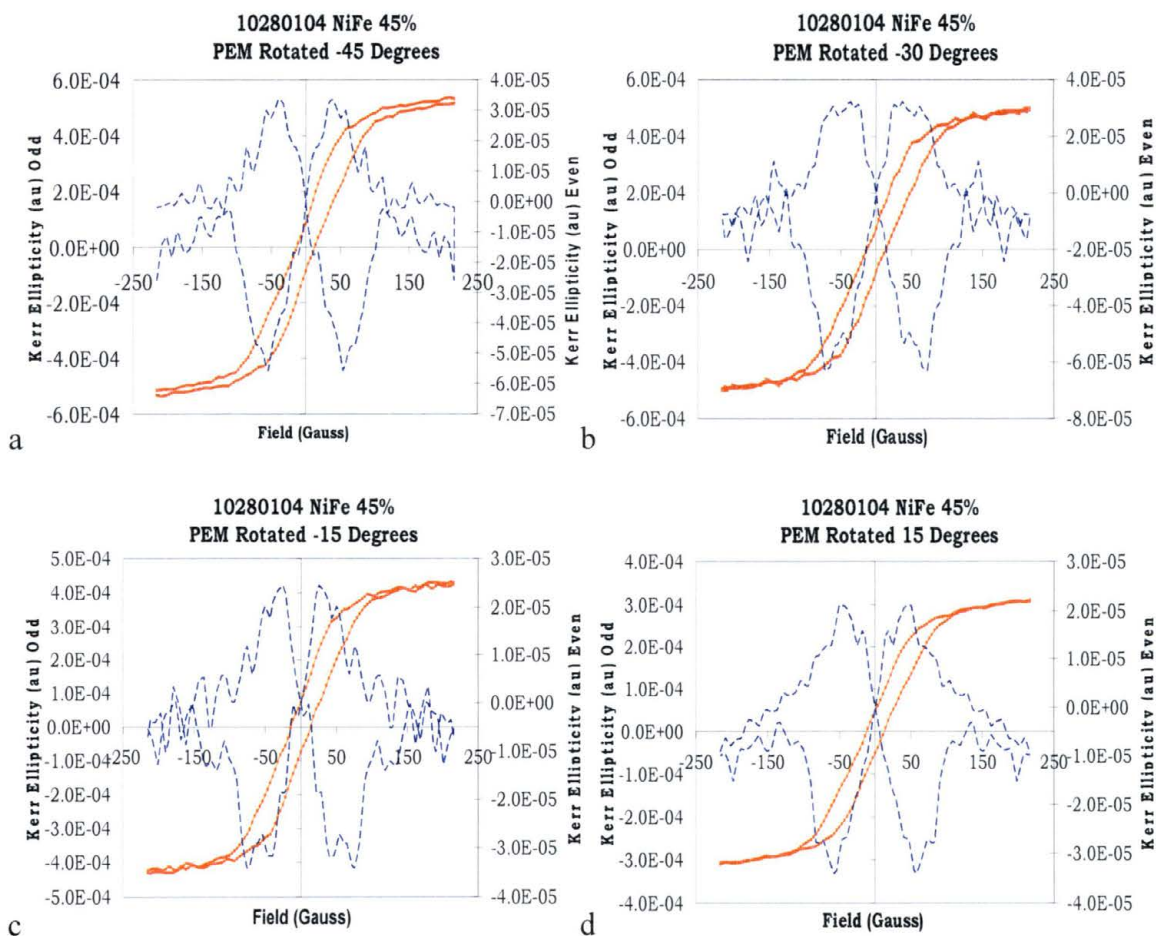
5.1.2.1 Separation of the Even and Odd Parts from the Curves

As stated earlier, we noticed that the curves show an asymmetrical appearance. We wrote a DOS based program that reads the text file of the curves, and separates the even from the odd parts and the result file is then used to create a new graph. Odd and even parts were calculated using the following algorithm:

$$M_{odd}(H) = \frac{1}{2}[M_{desc}(H) - M_{ascending}(-H)] \quad (5.1)$$

$$M_{even}(H) = \frac{1}{2}[M_{desc}(H) + M_{ascending}(-H)] \quad (5.2)$$

The source code on the program is listed in Appendix A. Each of these graphs show two curves. The first curve is a curve that looks like a typical odd hysteresis curve (solid line) and the second curve is the even part of the hysteresis curve. Figure 5.5 shows the Kerr ellipticity graphs and figure 5.6 the Kerr rotation graphs.



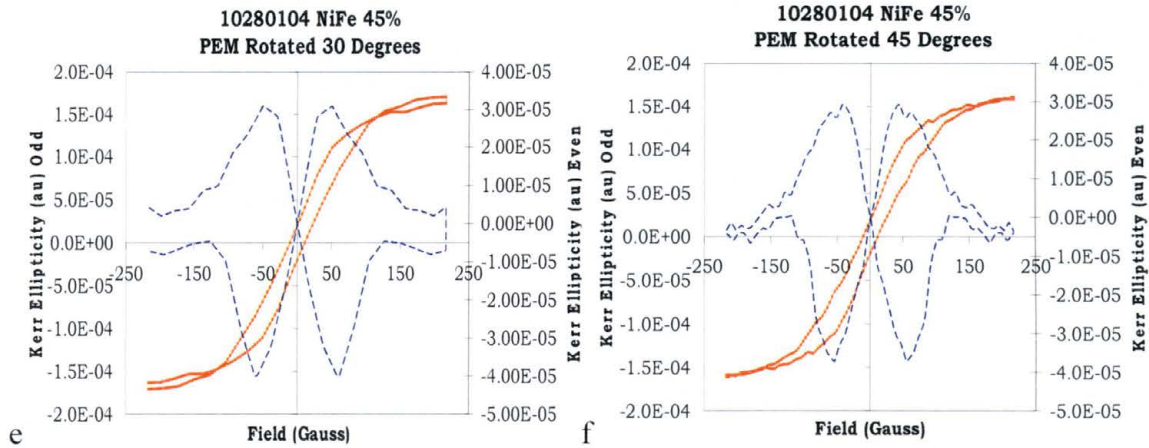
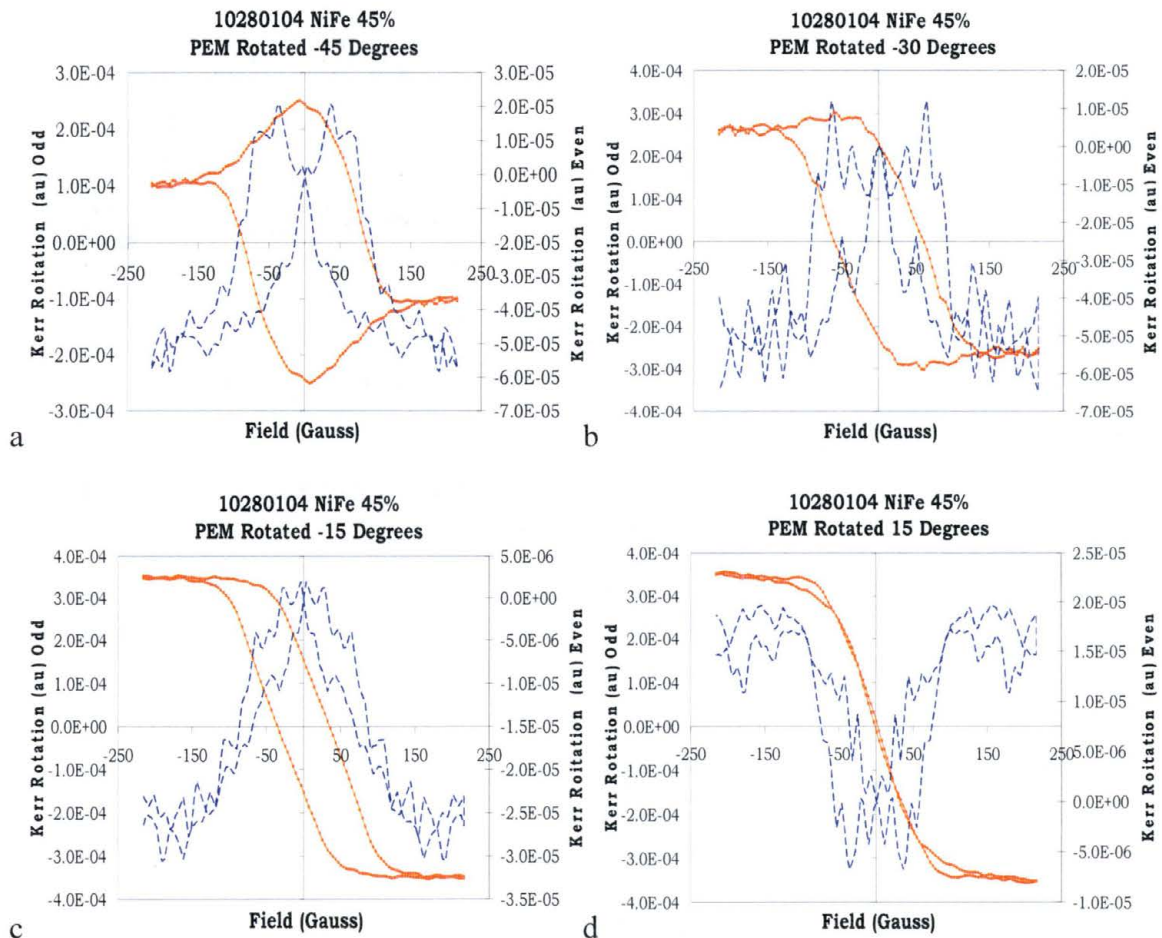


Figure 5.5 Odd and even parts of the Kerr ellipticity hysteresis curve of sample 10280104 for different orientations of the PEM: (a) -45 degrees; (b) -30 degrees; (c) -15 degrees; (d) 15 degrees; (e) 30 degrees; (f) 45 degrees



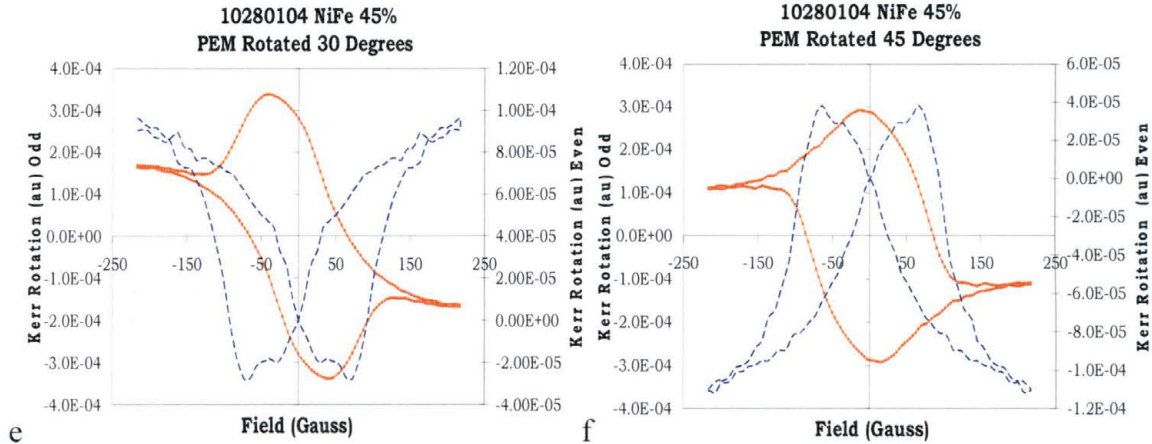


Figure 5.6 Odd and even parts of the Kerr rotation hysteresis curve of sample 10280104 for different orientations of the PEM: (a) -45 degrees; (b) -30 degrees; (c) -15 degrees; (d) 15 degrees; (e) 30 degrees; (f) 45 degrees

We suggest that the odd functions correspond to the traditional Kerr signals and are due to non-diagonal components of the effective dielectric tensor. It was shown in chapter 3 that these non-diagonal components are to a first approximation linear functions of the molecular field and magnetization. The even functions in Figures 5.5 and 5.6 are due to the M -dependence of the diagonal components of the effective dielectric tensor. It was shown in chapter 3 that the diagonal components of the dielectric tensor are an even function of the magnetization. Looking at Fig. 5.5 it appears that the odd part of the ellipticity hysteresis curve is almost independent of the orientation of the PEM. Figure 5.6, however, shows that the odd part of the rotation hysteresis curve depends strongly on the orientation of the PEM.

When looking at the even part in each graph in Figure 5.5, we see that there is a correlation with the magnitude of the even part and the angle of the PEM. The magnitudes are greatest (approximately $10 \cdot 10^{-5}$ between the extremes) when the PEM is rotated to -45° and 45° and is reduced to almost half (approximately $6.5 \cdot 10^{-5}$ between the extremes) when it is rotated to -15° . If we look at Figure 5.6 it is the same way. We can see a correlation between the magnitudes of the even parts and the angle of the PEM. The difference between the extremes is from 10^{-4} with the PEM rotated to 45° to $9 \cdot 10^{-5}$ with the PEM rotated to -45° . The rotation with the smallest difference is at 15° , and the separation of the extremes of the even part is approximately $3 \cdot 10^{-5}$. We also notice that there seems to be some periodicity in the even parts of both the rotation and ellipticity graphs. We are not sure if this is just noise, or if there is a signal being introduced there. If I wanted to make a measurement where the contribution from the diagonal components in the effective dielectric tensor is the smallest, then I would take measurements with the PEM rotated to 15° using the 2ω signal (Kerr rotation signal).

If we look at Figures 5.4 through 5.6, we can conclude that the origin of the negative susceptibility cannot be caused by the diagonal components of the effective dielectric tensor. The odd part of the MO-Kerr hysteresis curve still contains the negative susceptibility. A negative susceptibility is not observed in the odd part of the M.O. Kerr Ellipticity curves. In the setup described in chapter 4, the PEM is placed

in front of the sample. This makes it difficult to know what the state of polarization (SOP) of the incident light is. If we also look to figure 3.2, the SOP of the light needs to be oriented such that the setup is only sensitive for the component of magnetization that we are looking for.

CHAPTER 6

NEW MEASUREMENT RECIPE

6.1 Selection of the in-plane component of the magnetization

As shown in chapter 3, the force on the free charge carriers is given by:

$$\vec{F} = q\vec{E} + q(\vec{v} \times \vec{B}_{MF}) \quad [6.1]$$

$$\vec{B}_{MF} \propto \vec{M} \quad [6.2]$$

where \mathbf{E} is the electric field component of the EM-wave, and \mathbf{B}_{MF} is the molecular field introduced in chapter 3. The motion of the charges is mainly caused by the \mathbf{E} . If we choose \mathbf{E} parallel to \mathbf{B}_{MF} , the 2nd component of equation [6.1] will be zero, and no linear or non-linear MO Kerr effects is observed. This is also explained in Fig. 3.2. So in order to measure only the component of the magnetization parallel to the applied magnetic field, it is necessary to use incident light that is linearly polarized perpendicular to the plane of incidence.

In Chapter 4, the ellipsometer setup was discussed. With the original setup, the PEM was attached to the polarizer, which is in

front of the sample. With the PEM in front of the sample, the state of polarization (SOP) of the light is modulated from left circular polarized light to right circular polarized light. This means that the light is not guaranteed to be polarized perpendicular to the plane on incidence. We solved this problem by placing the PEM between the sample and the analyzer which allows the SOP of the incident light to be linearly polarized in the direction that we choose it to be. In this case we want the light to be perpendicular to the plane of incidence. Figure 6.1 shows the new ellipsometer setup.

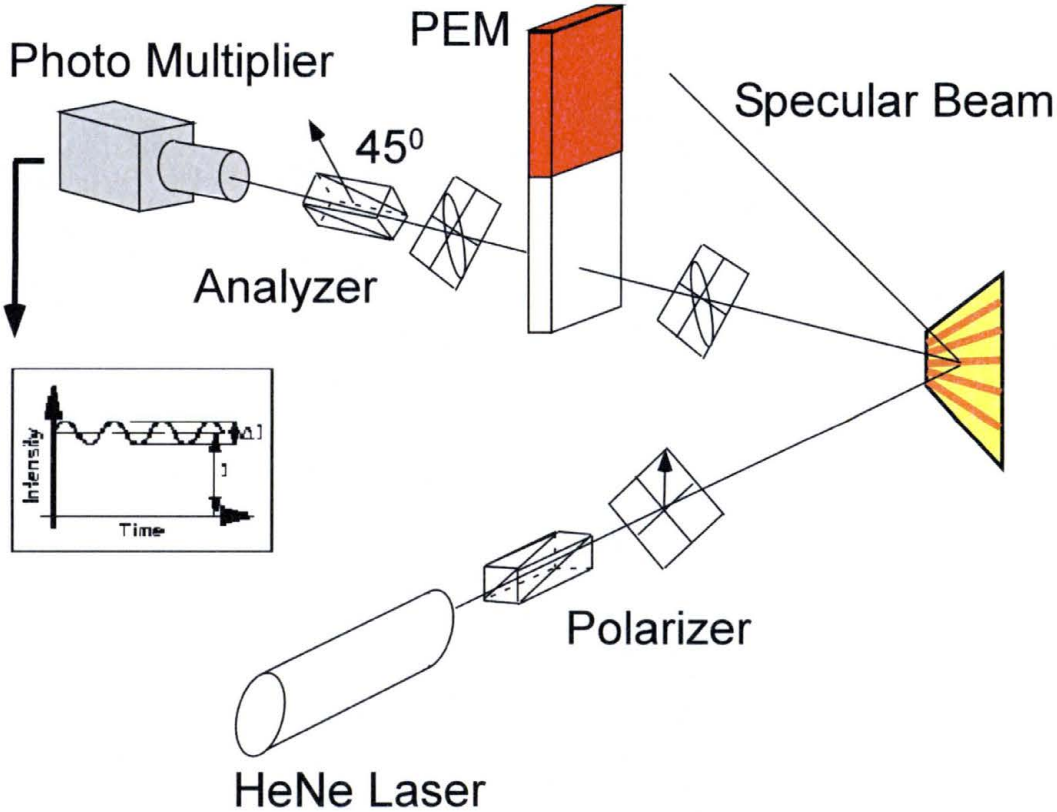


Figure 6.1 New Measurement Setup

6.1.1 Longitudinal Magnetization Component

By rotating the polarizer to where its polarization axis is vertical such that it is perpendicular to the plane of incidence, we can minimize the sensitivity for the transverse magnetization component and in turn maximize the sensitivity for the longitudinal magnetization component. This means that the Kerr effect that is noticed when the analyzer is rotated such that the signal is minimized is caused only by the longitudinal magnetization component. Fig. 6.2 shows the hysteresis curve for the Kerr rotation vs. applied magnetic field measured for this configuration. The magnetic field was applied perpendicular to the strips. No negative susceptibilities as shown in chapter 5 are observed.

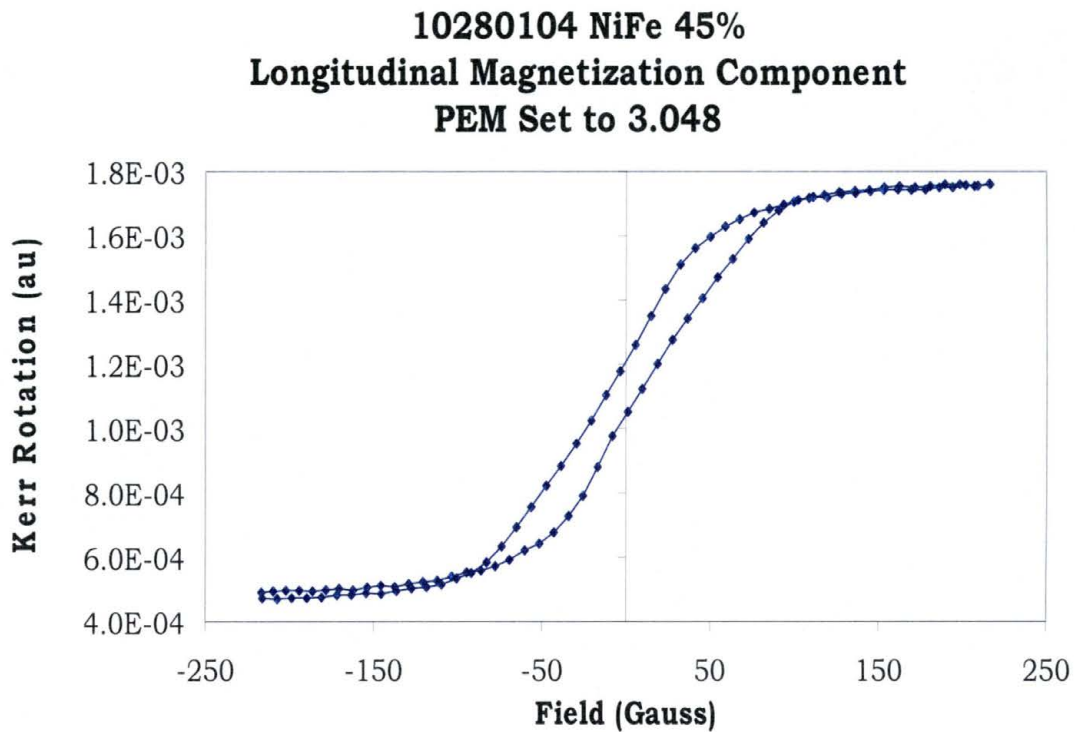


Figure 6.2 Longitudinal hysteresis curve of sample 10280104 (component of the magnetization parallel to the applied field) from the large grating

The material reaches saturation at approximately 100 Gauss and has a small coercivity. The graph is symmetrical.

6.1.2 The Transverse Magnetization Component

To see the transverse magnetization component, the polarizer is rotated so that its axis is in a horizontal position. This means that the plane of polarization of the incident wave is parallel to the applied magnetic field. In this case, the sensitivity for the longitudinal

magnetization component is minimized but not equal to zero. Measurements are done with the analyzer rotated to a vertical position. Figure 6.3 is the hysteresis curve for the transverse magnetization component.

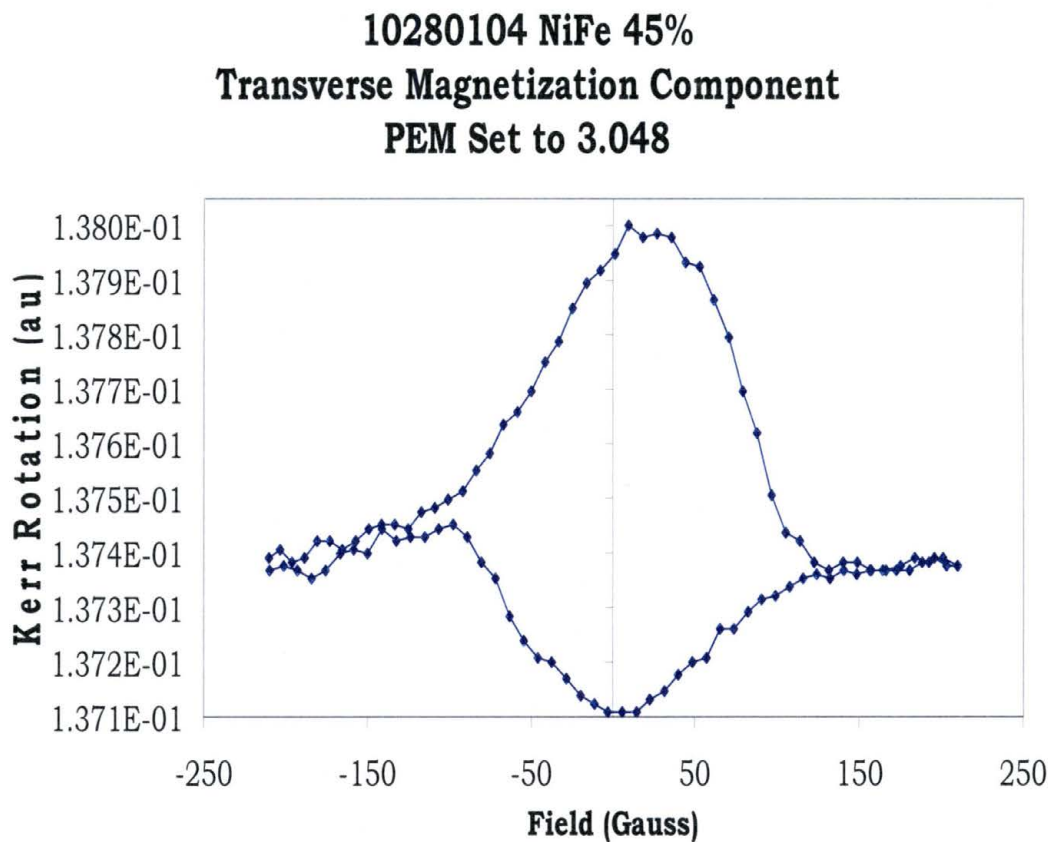


Figure 6.3 Transverse hysteresis curve of sample 10280104 (component of the magnetization perpendicular to the applied field) from the large grating

The coercivity, or reversal field, for this component is much larger than for the longitudinal component. This is due to the fact that measurement was done on a grating that has an easy axis and a hard axis for the magnetization. The easy axis of the gratings is

parallel to the strips while the hard axis is perpendicular to the strips and thus parallel to the applied field. If no magnetic field is applied to this sample, then the magnetization will line up along the easy axis of the sample. If the sample is perfectly aligned with the easy axis exactly perpendicular to the externally applied magnetic field, we would expect that half of the strips would be magnetized up and half of the strips would be magnetized down. Since the transverse hysteresis curve of Fig. 6.3 shows a large remanence, it is clear that the sample is not perfectly aligned with its easy axis perpendicular to the applied magnetic field.

6.2 Non-linear Component of the Magnetization.

It is noticeable that the graph of the transverse component is not symmetrical. The reason for this can be attributed to the non-linear effects outlined in chapter 3. At this moment it is not clear how to adapt the measurement technique to avoid those non-linear effects. Of course it is possible to separate the odd and the even parts of the hysteresis curve using the mathematical techniques as shown in chapter 5.

6.3 The Kerr Microscope Measurement Results

In order to check the new measurement setup, domain analysis has been performed on sample 10250101 using the MO Kerr microscope of the University of Twente. The results of this domain analysis have been used to calculate the hysteresis curve. Those calculated curves were compared to the curves measured with the MO Kerr tracer. The incident light was polarized perpendicular to the plane of incidence which makes the setup only sensitive for the longitudinal component of the magnetization. An in-plane magnetic field was applied parallel to the strips of the sample. After the data was collected, we analyzed each set of pictures and calculated the hysteresis curve from the domain images. The following subsections address the method for calculating the curves.

6.3.1 The Large Grating

The procedure used to gather the information from the large grating was fairly simple. Figure 6.4 shows a picture from the large grating. When looking at this picture, there are three shades to look at to determine what is happening in the film. They are “A” the Si

substrate, “B” the NiFe film with the domains in the right direction, and “C” the NiFe film with the domains in the opposite direction

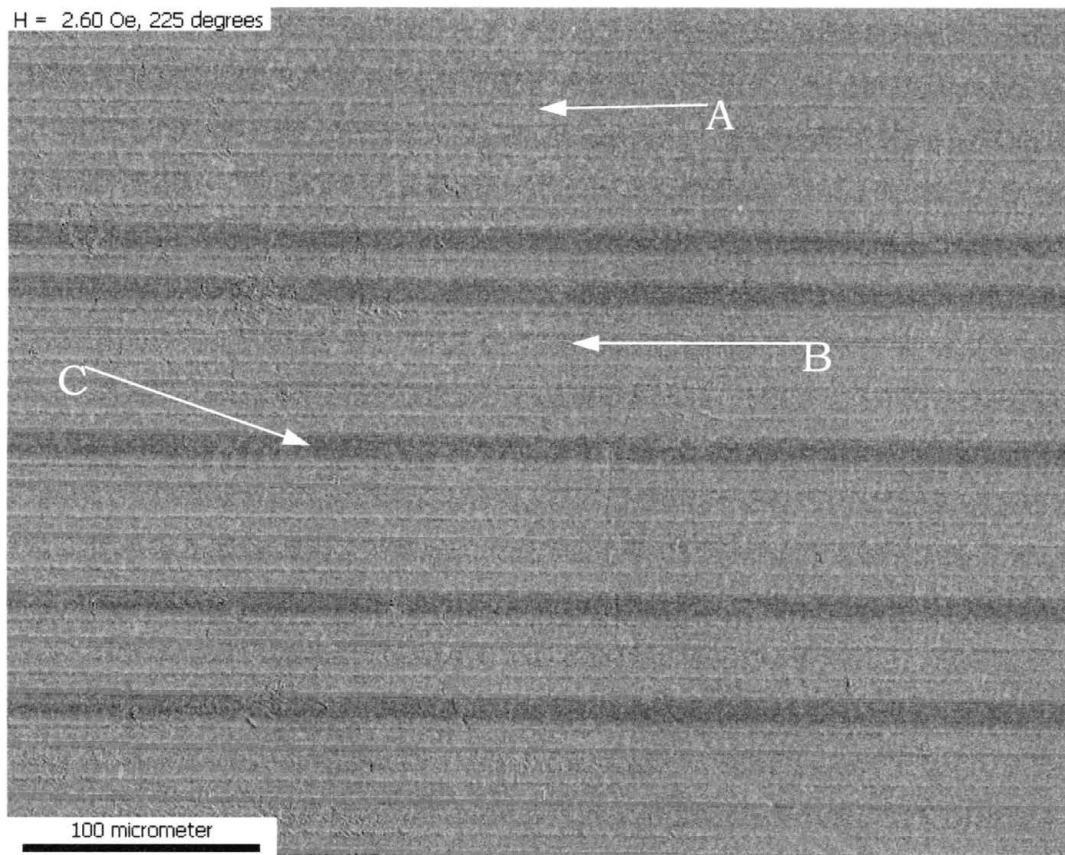


Figure 6.4 The Large Grating

The collection procedure started when all of the domains were aligned in the “B” direction. As the magnetic field was increased, the strips would flip. This means that the whole strip would flip at the same time. The process of creating a hysteresis curve consisted of recording each number of strips that flip versus the applied field. Once the sample was saturated, the sample was rotated 180° and the

field was then increased until all of the domains had flipped again. Figure 6.5 is a picture of the sample while it was undergoing the reversal process. The labels “A”, “B”, and “C” are the same as before.

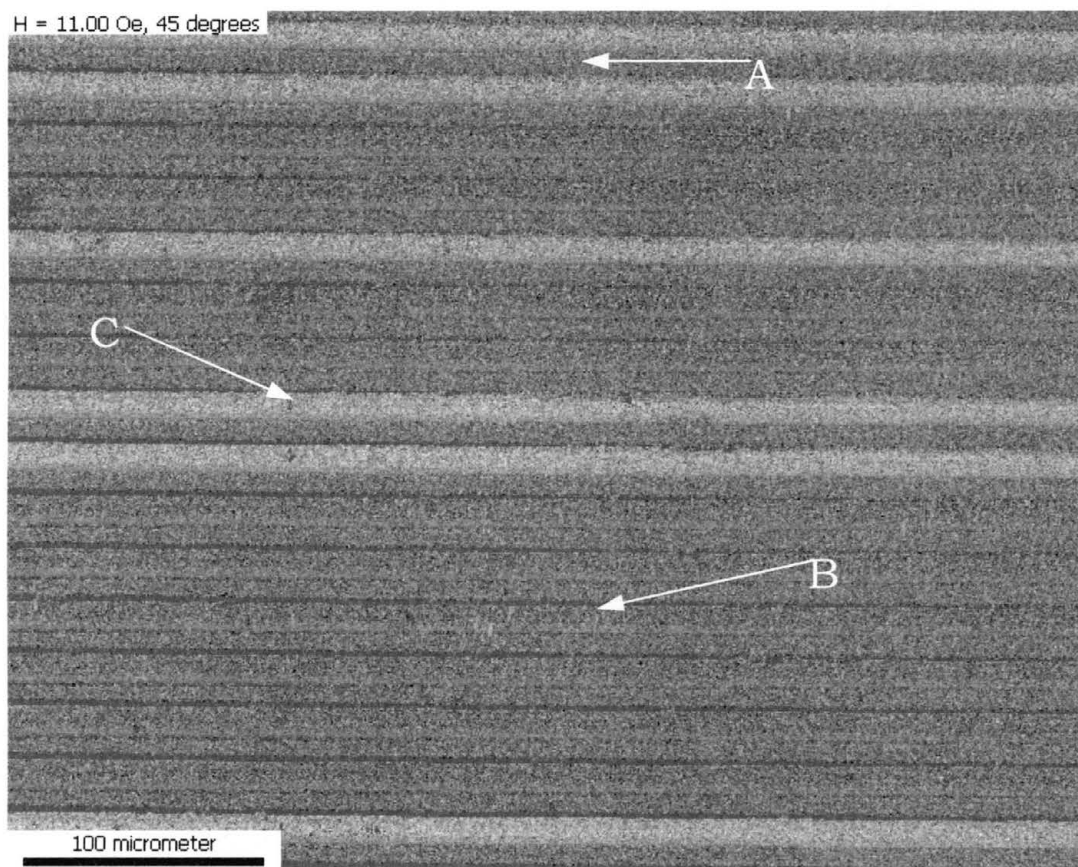


Figure 6.5 The Large Grating During Reversal Process

Once the data was collected, a hysteresis curve was created. Figure 6.6 shows this curve. The blue curve (Diamonds) represents the first set of data from the applied field, and the red curve (Squares) represents the data from the applied field with the sample turned 180° . The coercivity of this curve is approximately 7 Oe. The period

for the large grating, as measured by Claude Garrett [5], is 18.25 μm and the line width is 10 μm .

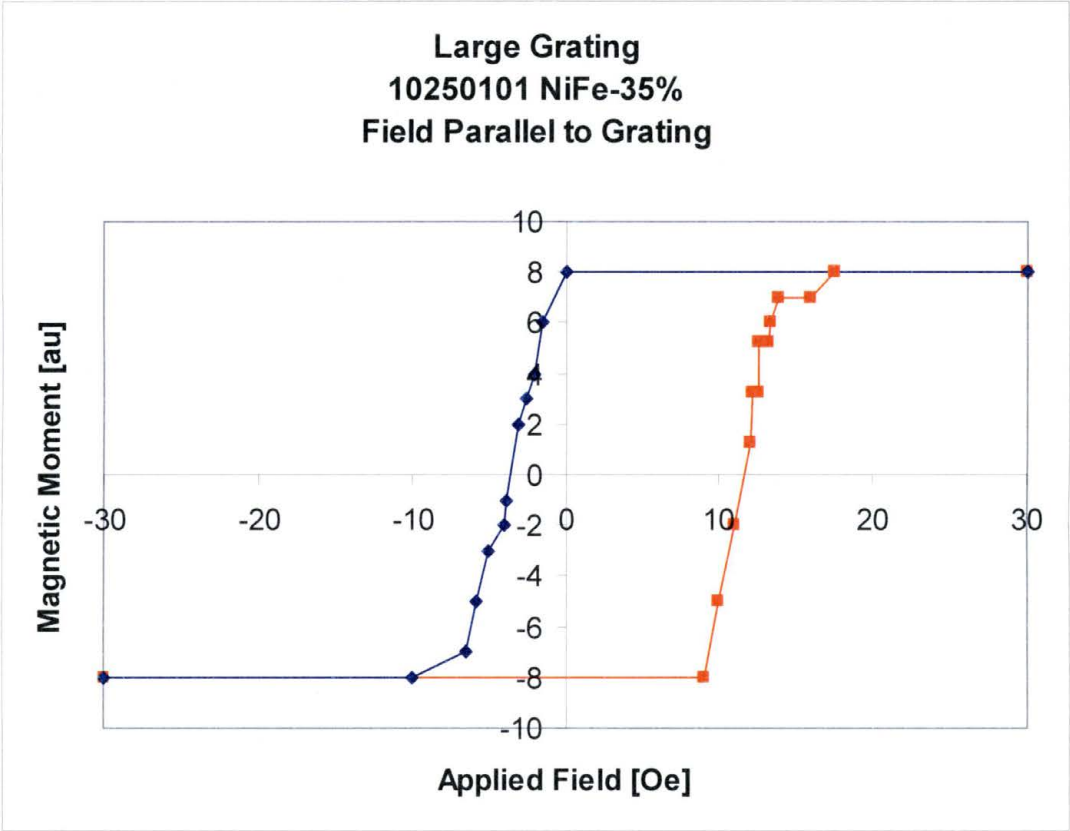


Figure 6.6 Large Grating Sample # 10250101

6.3.2 The Medium Grating

The procedure for the data collected for this grating was the same as the procedure for the large grating with the exception that when I calculated the number of lines of domains that flipped I had to measure some lines that did not flip all of the way. When recording this data, I took the length of the line and divided this length by the

total length of the grating from the picture. This gave me a nice ratio to use for recording the data. Figure 6.7 shows a picture where this situation occurred.

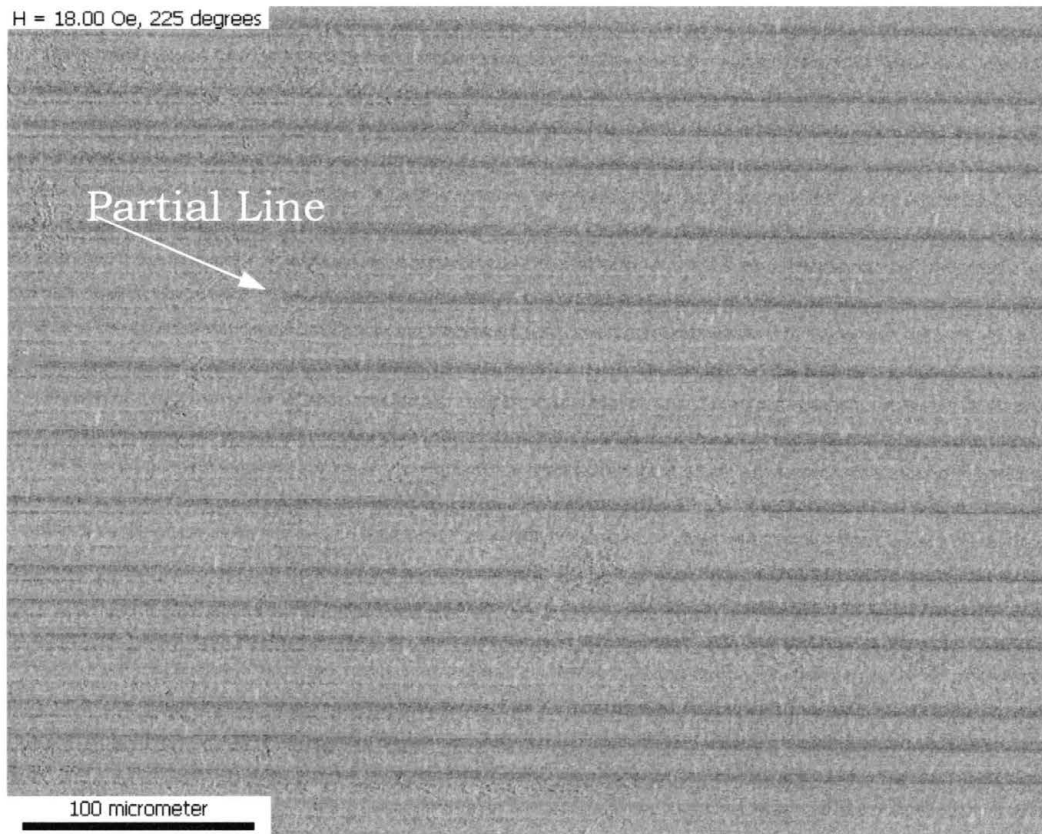


Figure 6.7 Medium Grating With Partially Flipped Strip

Figure 6.8 is the hysteresis curve for the medium grating. The coercivity for this grating is approximately 17 Oe. The blue curve (Triangles) represents the first set of data from the applied field, and the red curve (Diamonds) represents the data from the applied field with the sample turned 180° . The period for this grating is $12.16 \mu\text{m}$ and the line width is $6 \mu\text{m}$.

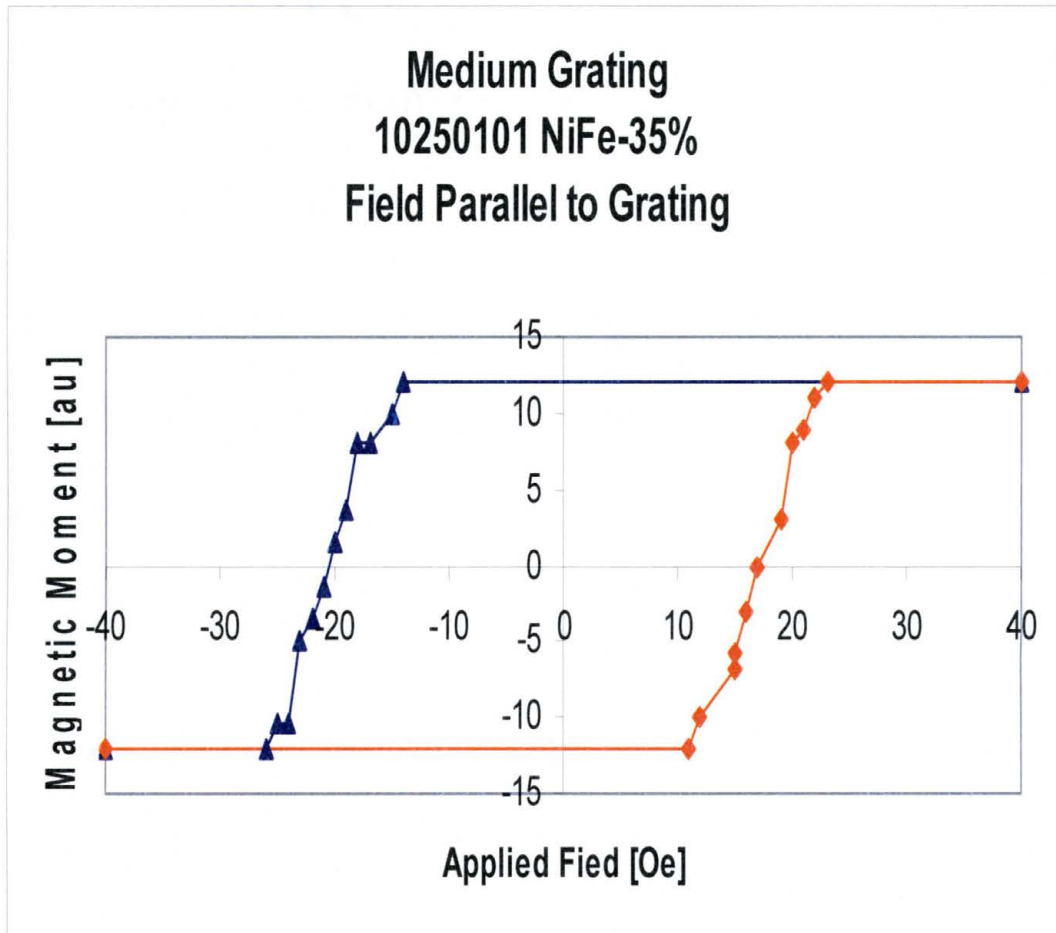


Figure 6.8 Medium Grating Sample # 10250101

6.3.3 The Small Grating

The method for obtaining the hysteresis curve for this grating was more involved. The reason for this is because of the size of the grating strips and the larger coercivity. It was rare that the total strip flip for a given change in magnetic field, as was the case for the large grating, so I came up with an idea to use AutoCad to help in measuring the lengths of the lines for each of the pictures. The

pictures were inserted into AutoCad and then the line command was used to trace each segment of the strip that had flipped. After the line tracing was completed, the images were rescaled using the scale on the bottom of the picture. This was done to ensure that all of the drawings would have the same scale so that they could be compared as the other two gratings were done. After the images were scaled, I ran a lisp program, which is a program written such that AutoCad can perform this task, that summed up all of the segments into a total length of flipped strips. Figures 6.9, 6.10, and 6.11 are three screen captures that were taken during this process. Each one in succession has an increase in number of red lines. These red lines are the line segments that were drawn on top of the image.

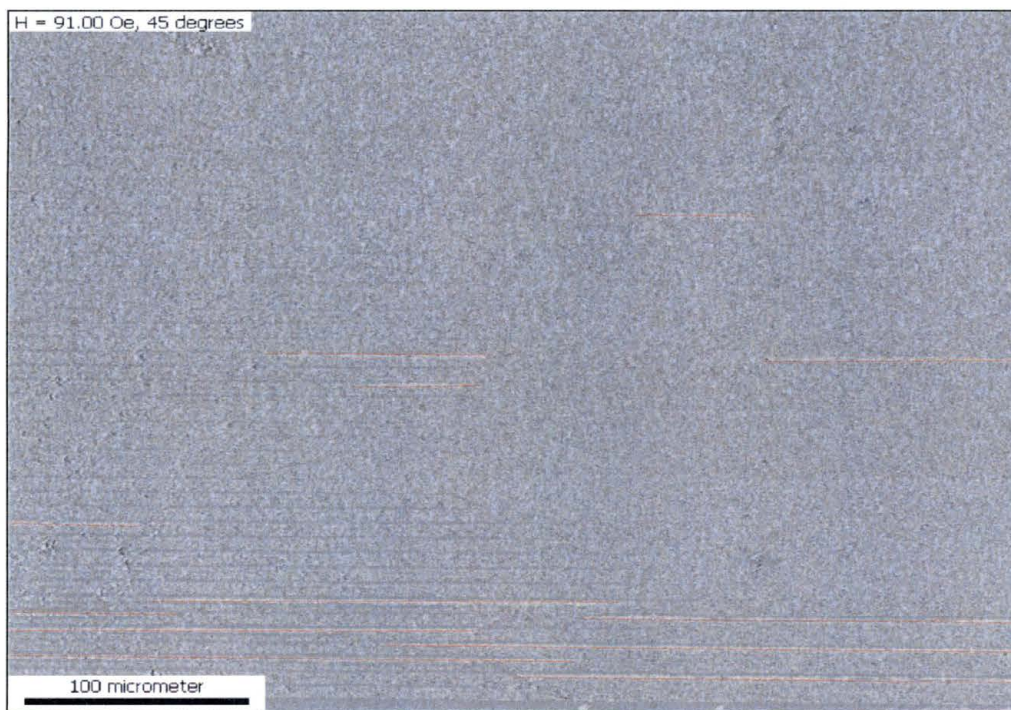


Figure 6.9 Small Grating Sample 10250101 1st Image

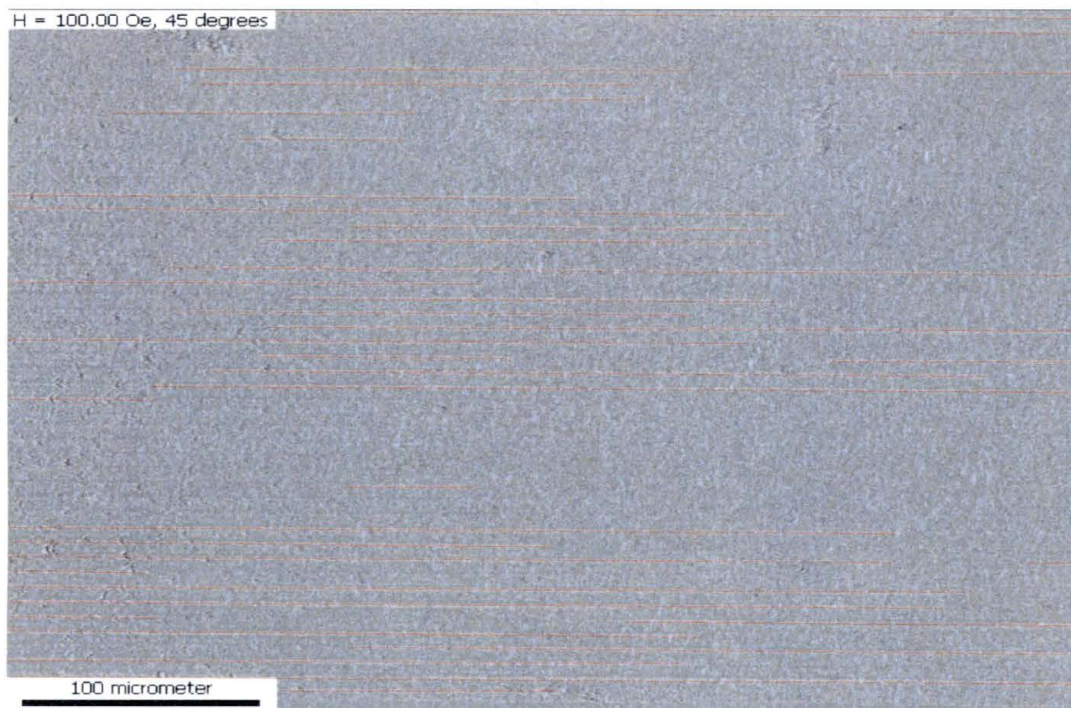


Figure 6.10 Small Grating Sample 10250101 2nd Image

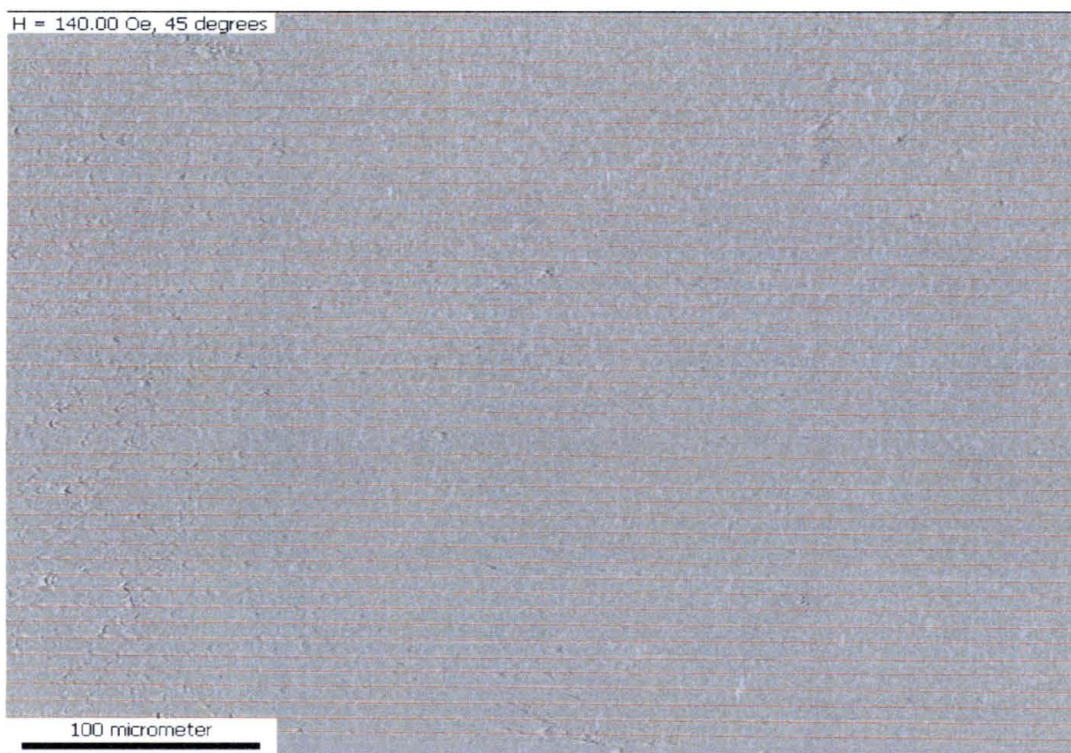


Figure 6.11 Small Grating Sample 10250101 3rd Image

After collecting the lengths for each image, I created a hysteresis curve which is shown in figure 6.12. The coercivity of this curve is approximately 100 Oe. The blue curve (Squares) represents the first set of data from the applied field, and the red curve (Diamonds) represents the data from the applied field with the sample turned 180° . The period for this grating is $6.1 \mu\text{m}$, and the line width is $1.5 \mu\text{m}$.

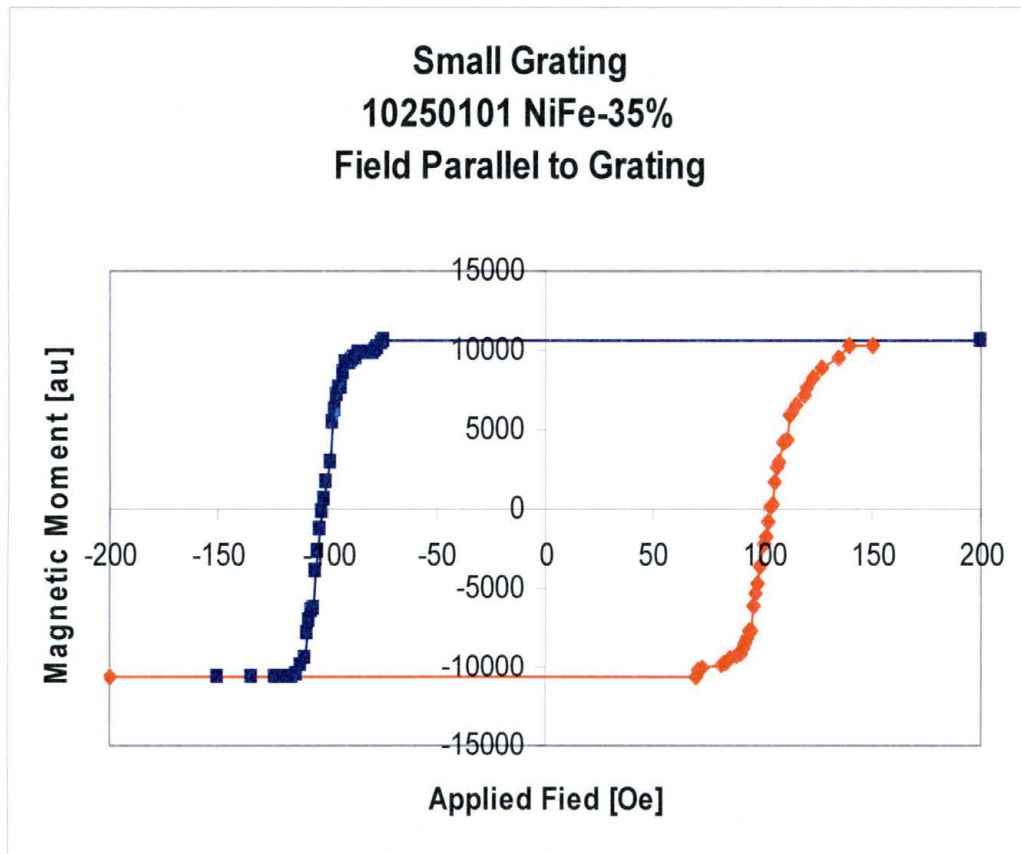


Figure 6.12 Small Grating Sample # 10250101

That the coercivities obtained using the Kerr Microscope are consistent with the coercivities measured using the MO Kerr tracer supports the new setup and measurement recipe.

CHAPTER 7

7. CONCLUSIONS AND RECOMMENDATIONS

7.1 Summary and Conclusions

In this thesis we were able to separate the two in-plane magnetization components using the Magneto-optical Kerr ellipsometer, and we were able to use the Kerr microscope to analyze the NiFe metal film to quantitatively measure the magnetic hysteresis of the film. We also determined that the negative susceptibility was coming from the transverse component of the magnetization.

We first had to characterize the ellipsometer setup and ensure that the PEM followed theory. We found that it did follow the theory, and that there was a small dependence on the angle in which the PEM was rotated when it was placed before the sample. We also determined that the best angle to rotate it would be 15° so that the contribution from the diagonal terms in the effective dielectric tensor will be small compared to the off-diagonal terms.

To be able to separate the components, we needed to ensure that the state of polarization of the light was in the direction that we wanted it

to be instead of being modulated between right circular and left circular polarization. We did this by placing the PEM behind the sample. By doing this we were able adjust the angle of the polarizer so that one of the magnetization components could be either cancelled out or minimized such that the only component we would see is that component that we are looking for. By placing the PEM behind the sample we were also able to minimize the asymmetric behavior (even part of the hysteresis curve) that we saw when the PEM was placed before the sample.

7.2 Recommendations for Further Research

7.2.1 Measuring the Medium and Small Grating

By measuring the medium and small gratings, the dependence of the hysteresis of the film can be determined as a function of the size of the microstructure. The behavior due to the anisotropy can also be investigated.

7.2.2 Dependence when the Magnetic Field is Applied Along Easy Axis

We performed the measurements with the ellipsometer with the magnetic field applied parallel to the film, and the gratings were aligned in a vertical position. The gratings can be placed in a horizontal position such that the easy axis is parallel with the applied magnetic field.

7.2.3 Applying Additional External Stresses

By applying an external stress, the strain in the film can change the hysteresis properties of the film, as shown by Patrick Holland [3]. With the new setup it should be possible to determine the magnetic hysteresis of the gratings as a function of an externally applied isotropic stress. Such investigation would contribute to a better understanding of the magneto-elastic properties of microstructured thin films.

APPENDIX A

Separation of Odd and Even Part of Hysteresis Curve.

The hysteresis curves have an even part and an odd part. Let us assume that the odd part is identified by $O(H)$ and the even part by $E(H)$.

So:

$$O(H) = -O(-H)$$

$$E(H) = E(-H)$$

Each hysteresis curve consists of an ascending branch and a descending branch. The ascending branch is the values measured when starting at a large negative field, decreasing the magnetic field to zero and then increasing the magnetic field in the positive direction until the sample is saturated along the positive field direction. The descending branch of the hysteresis curve is the values measured when starting at large positive field, decreasing the magnetic field to zero and then increasing the magnetic field in the negative direction until the sample is saturated along the negative field direction. So we have two functions:

$$M_{ascending}(H) = O(H - H_c) + E(H - H_c)$$

$$M_{descending}(H) = O(H + H_c) + E(H + H_c)$$

We used the following algorithm to separate the odd and the even parts:

$$\begin{aligned} & \frac{1}{2}(M_{ascending}(H) + M_{descending}(-H)) = \\ & \frac{1}{2}(O(H - H_c) + E(H - H_c) + O(-H + H_c) + E(-H + H_c)) = \\ & \frac{1}{2}(O(H - H_c) + E(H - H_c) - O(H - H_c) + E(H - H_c)) = E(H - H_c) \\ & \frac{1}{2}(M_{ascending}(H) - M_{descending}(-H)) = \\ & \frac{1}{2}(O(H - H_c) + E(H - H_c) - O(-H + H_c) - E(-H + H_c)) = \\ & \frac{1}{2}(O(H - H_c) + E(H - H_c) + O(H - H_c) - E(H - H_c)) = O(H - H_c) \end{aligned}$$

All measured hysteresis curves were shifted along the y-axis.

The source code of the c++ program written by Dr. Geerts is given below:

```
// JettHendrix.cpp : Defines the entry point for the console application.
//

#include "stdafx.h"

#include<fstream.h>
#include<string.h>

#include<iomanip.h>

int main()
{
    ifstream datafile;
    ofstream output;
    char infilename[200];
    char outfilename[200];
    char item[200];
```

```

int numpoints;
int num, highpointer,lowpointer,multipl;
int ii,jj,maxii, maxdesc, maxasc, resmaxdesc, resmaxasc;
double field[300], fieldasc[150], fielddes[150], resfieldasc[150],
resfielddes[150];
double magnetization[300], magnetizationdes[150],
resmagnetizationdes[150], magnetizationasc[150],
resmagnetizationasc[150];
double maxfield, CurrentField;
cout << "Calculations of Symmetric and Asymmetric Part of the
Hysteresis curve\n";
cout << "Jett Hendrix / Wilhelmus Geerts, Southwest Texas State
University\n";
cout << "Summer 2002\n\n";
cout << "What is the name of the Kerr data file? \n";
cout << "I will skip the first 15 lines and look for the line with the
[begin] label. \n";
cout << "I will only look for the first two collumns. \n";
cout << "I will read all the way until I find the [end] label. \n";
cout << "File name please: ";
cin >> infilename;

datafile.open(infilename, ios::in); //Need safeguards here

cout <<"\nI will write the original data to the output file.\n";
cout <<"I will resample the data (2x120 points).\n";
cout << "I will write the resampled data to the output file.\n";
cout <<"I will calculate the assymetric and symmetric parts of the
hysteresis curves.\n";
cout <<"Both parts will be centered around zero and written to the
output file.\n";
cout << "What is the name of the output file: ";
cin >> outfile;
output.open(outfile, ios::out); //Need safeguards here

cout << "Processing Header...";
ii=1;
while (ii!=15)
{
    datafile.getline(item, 200, '\n');
    output << item;
    output << "\n";
    ii=ii+1;
}

datafile >> item; //Record type, ignore for now

```

```

while (strcmp(item,"[begin]")!=0 && (datafile.peek()!=EOF))
{datafile >> item;
  cout << item;
  cout << "\n";
  output << item;
}

cout << "Found Begin of data\n";
cout << item;
  output << item;
  cout << "\nReading hysteresis data\n";
  output << "\nReading hysteresis data\n";
ii=1;
  while( (datafile.peek()!='\n'))
  {
    datafile >> field[ii];
  datafile >> magnetization[ii];
    cout << field[ii];
    cout << " ";
    cout << magnetization[ii];
    cout << "\n";
    output << field[ii];
    output << " ";
    output << magnetization[ii];
    ii=ii+1;
    datafile.getline(item, 200, '\n');
    output << item;
    output << "\n";

  }
maxii=ii-1;
ii=1;
multipl=1;
if (field [1]<0)
{
  multipl=-1;
  while (ii<=maxii)
  {
    field[ii]=-field[ii];
    ii=ii+1;
  }
}
cout <<"Total number of data points: ";
cout << maxii;
cout << "\n";

```



```

    cout << maxfield/60;
    cout << "\n";
output << "Resampling Descending Branch between: ";
    output << maxfield;
    output << " and ";
    output << -maxfield;
    output << " in steps of ";
    output << maxfield/60;
    output << "\n";
    CurrentField=maxfield;
    highpointer=1;
    lowpointer=2;
    ii=1;
    while (CurrentField>=-maxfield)
    {
        while (CurrentField<=fielddes[lowpointer] &&
lowpointer<=maxdesc) lowpointer=lowpointer+1;
        while (CurrentField<=fielddes[highpointer] &&
highpointer<=maxdesc+1) highpointer=highpointer+1;
        if (highpointer !=1) highpointer=highpointer-1;
        resfielddes[ii]=CurrentField;
        if (CurrentField == fielddes[highpointer])
        { resfielddes[ii]=fielddes[highpointer];
          resmagnetizationdes[ii]=magnetizationdes[highpointer];
        }
        else
        { resfielddes[ii]=CurrentField;

resmagnetizationdes[ii]=magnetizationdes[lowpointer]+(magnetizationdes[
highpointer]-magnetizationdes[lowpointer])/(fielddes[highpointer]-
fielddes[lowpointer])*(CurrentField-fielddes[lowpointer]);
        }
        cout << resfielddes[ii]*multipl;
        cout << " ";
        cout << resmagnetizationdes[ii];
        cout << "\n";
        output << resfielddes[ii]*multipl;
        output << " ";
        output << resmagnetizationdes[ii];
        output << "\n";
        ii=ii+1;
        CurrentField=CurrentField-maxfield/60;
    }
    CurrentField=-maxfield;
    while (CurrentField<=fielddes[lowpointer] &&
lowpointer<=maxdesc) lowpointer=lowpointer+1;

```

```

        while (CurrentField<=fielddes[highpointer] &&
highpointer<=maxdesc+1) highpointer=highpointer+1;
        if (highpointer !=1) highpointer=highpointer-1;
        resfielddes[ii]=CurrentField;
        if (CurrentField == fielddes[highpointer])
            { resfielddes[ii]=fielddes[highpointer];
              resmagnetizationdes[ii]=magnetizationdes[highpointer];
            }
        else
            { resfielddes[ii]=CurrentField;

resmagnetizationdes[ii]=magnetizationdes[lowpointer]+(magnetizationdes[
highpointer]-magnetizationdes[lowpointer])/(fielddes[highpointer]-
fielddes[lowpointer])*(CurrentField-fielddes[lowpointer]);
        }
        cout << resfielddes[ii]*multipl;
        cout << " ";
        cout << resmagnetizationdes[ii];
        cout << "\n";
        output << resfielddes[ii]*multipl;
        output << " ";
        output << resmagnetizationdes[ii];
        output << "\n";
        resmaxdesc=ii-1;
        ii=ii+1;
        cout << "Resampling Ascending Branch between: ";
        cout << -maxfield;
        cout << " and ";
        cout << maxfield;
        cout << " in steps of ";
        cout << maxfield/60;
        cout << "\n";
        output << "Resampling Ascending Branch between: ";
        output << -maxfield;
        output << " and ";
        output << maxfield;
        output << " in steps of ";
        output << maxfield/60;
        output << "\n";
        CurrentField=-maxfield;
        lowpointer=1;
        highpointer=2;
        ii=1;
        while (CurrentField<=maxfield)
        {

```

```

        while (CurrentField>=fieldasc[highpointer] &&
highpointer<=maxasc+1) highpointer=highpointer+1;
        while (CurrentField>=fieldasc[lowpointer] &&
lowpointer<=maxasc) lowpointer=lowpointer+1;
        if (lowpointer !=1) lowpointer=lowpointer-1;
        resfieldasc[ii]=CurrentField;
        if (CurrentField == fieldasc[lowpointer])
        { resfieldasc[ii]=fieldasc[lowpointer];
          resmagnetizationasc[ii]=magnetizationasc[lowpointer];
        }
    else
        { resfieldasc[ii]=CurrentField;

resmagnetizationasc[ii]=magnetizationasc[lowpointer]+(magnetizationasc[
highpointer]-magnetizationasc[lowpointer])/(fieldasc[highpointer]-
fieldasc[lowpointer])*(CurrentField-fieldasc[lowpointer]);
    }
        cout << resfieldasc[ii]*multipl;
        cout << " ";
        cout << resmagnetizationasc[ii];
        cout << "\n";
        output << resfieldasc[ii]*multipl;
        output << " ";
        output << resmagnetizationasc[ii];
        output << "\n";
        ii=ii+1;
        CurrentField=CurrentField+maxfield/60;
    }
    CurrentField=maxfield;
    while (CurrentField>=fieldasc[highpointer] &&
highpointer<=maxasc+1) highpointer=highpointer+1;
    while (CurrentField>=fieldasc[lowpointer] && lowpointer<=maxasc)
lowpointer=lowpointer+1;
    if (lowpointer !=1) lowpointer=lowpointer-1;
    resfieldasc[ii]=CurrentField;
    if (CurrentField == fieldasc[lowpointer])
    { resfieldasc[ii]=fieldasc[lowpointer];
      resmagnetizationasc[ii]=magnetizationasc[lowpointer];
    }
    else
    { resfieldasc[ii]=CurrentField;

resmagnetizationasc[ii]=magnetizationasc[lowpointer]+(magnetizationasc[
highpointer]-magnetizationasc[lowpointer])/(fieldasc[highpointer]-
fieldasc[lowpointer])*(CurrentField-fieldasc[lowpointer]);
    }
}

```

```

cout << resfieldasc[ii]*multipl;
cout << " ";
cout << resmagnetizationasc[ii];
cout << "\n";
output << resfieldasc[ii]*multipl;
output << " ";
output << resmagnetizationasc[ii];
output << "\n";
ii=ii+1;
resmaxasc=ii-1;
cout << "\n\nThe asymmetric and symmetric parts of the hysteresis
curve: \n";
output << "\n\nThe asymmetric and symmetric parts of the
hysteresis curve: \n";
ii=1;
while (ii<=resmaxasc)
{
    cout << resfielddes[ii]*multipl;
    cout << " ";
    cout << (resmagnetizationdes[ii]+resmagnetizationasc[ii])/2;
    cout << " ";
    cout << (resmagnetizationdes[ii]-resmagnetizationasc[ii])/2;
    cout << "\n";
    output << resfielddes[ii]*multipl;
    output << " ";
    output << (resmagnetizationdes[ii]+resmagnetizationasc[ii]-
resmagnetizationdes[61]-resmagnetizationasc[61])/2;
    output << " ";
    output << (resmagnetizationdes[ii]-
resmagnetizationasc[ii])/2;
    output << "\n";
    ii=ii+1;
}
ii=1;
while (ii<=resmaxasc)
{
    cout << -resfielddes[ii]*multipl;
    cout << " ";
    cout << (resmagnetizationdes[ii]+resmagnetizationasc[ii])/2;
    cout << " ";
    cout << (-resmagnetizationdes[ii]+resmagnetizationasc[ii])/2;
    cout << "\n";
    output << -resfielddes[ii]*multipl;
    output << " ";
    output << (resmagnetizationdes[ii]+resmagnetizationasc[ii]-
resmagnetizationdes[61]-resmagnetizationasc[61])/2;

```

```
        output << " ";
        output << (-
resmagnetizationdes[ii]+resmagnetizationasc[ii])/2;
        output << "\n";
        ii=ii+1;
    }
    output << "\n Assymetric part shifted by: ";
    output << (resmagnetizationdes[61]+resmagnetizationasc[61])/2;
    output << "\n";
    output.close();
    datafile.close();
return 0;
}
```

Works Cited

- [1] S. N. Jasperson and S. E. Schnatterly, "An Improved Method for High Reflectivity Ellipsometry Based on a New Polarization Modulation Technique", *Rev. Sc. Instrum.* 40 (1969) 761.
- [2] Harland G. Tompkins, William A. McGahan, "Spectroscopic Ellipsometry and Reflectometry", 1999, John Wiley & Sons, New York.
- [3] Patrick Holland, "Magnetic Hysteresis Curves of Thin Films under Isotropic Stress", May 2001, Thesis Texas State University, San Marcos.
- [4] Brian Donehew, "Experimental setup for measuring the magneto-optical Kerr effect under high isotropic pressure", December 2001, Thesis, Texas State University, San Marcos.
- [5] Claude Garrett, "Fabrication and magnetic properties of patterned thin films", May 2002, Thesis, Texas State University, San Marcos.
- [6] K. Sato, "Measurement of Magneto-Optical Kerr Effect Using Piezo-Birefringent Modulator", *Jap. J. Appl. Phys.* 20 (1981) 2403.
- [7] William van Drent, CoNi/Pt multilayers for magneto-optical recording, January 1995, PhD. Thesis University of Twente, The Netherlands.
- [8] L. Callegaro, E. Puppini, "Isotropic in-plane external stressing of ferromagnetic films", *IEEE Trans. on Magn.* 32 (1996) 1065.

- [9] Dr. Alex Hubert, Dr. Rudolf Schäfer, “Magnetic Domains: The analysis of Magnetic Microstructures”, (1998) 41.
- [10] Hilda W.F. Sung, Czeslaw Rudowicz, “A Closer look at the Hysteresis Loop for Ferromagnets”, <http://arxiv.org/ftp/cond-mat/papers/0210/0210657.pdf>, 7.
- [11] Ron Atkinson “Magnetism in a New Light”, Hinds Instruments, INC. PEM Applications News for Users of Photoelastic Modulators, (Fall 2001). 2.
- [12] Casper Doppen, “The Designing and Building of a Kerr Microscope”, September 2003, Thesis, University of Twente.
- [13] <http://www.phase-shift.com/profilometer.html>
- [14] “Introduction to Magnetic Materials”, B.D. Cullity, Addison-Wesley, 1972, London.

VITA

Jett David Hendrix was born in San Angelo, Texas, on August 7, 1975, the son of Sharon Turn Hendrix and Paul Gail Hendrix, Sr. After graduating from San Marcos High School, San Marcos, Texas, in 1993 he entered Texas State University-San Marcos. He received his Bachelor of Science from Texas State University-San Marcos in May 2001. While completing his B.S. Physics degree, Jett worked as a lab instructor for the university. While in graduate college, he also taught labs at the university and during his last semester he worked as an applications intern for Jordan Valley Semiconductors, INC

Permanent Address: 13 Briarwood Dr.
 San Marcos, Texas 78666

This thesis was typed by Jett David Hendrix.